

1 Long-Range Transport Mechanisms in East and Southeast Asia and Impacts on Size-Resolved
2 Aerosol Composition: Contrasting High and Low Aerosol Loading Events
3
4

5 Rachel A. Braun¹, Mojtaba Azadi Aghdam¹, Paola Angela Bañaga^{2,3}, Grace Betito³, Maria
6 Obiminda Cambaliza^{2,3}, Melliza Templonuevo Cruz^{2,4}, Genevieve Rose Lorenzo², Alexander B.
7 MacDonald¹, James Bernard Simpas^{2,3}, Connor Stahl¹, Armin Sorooshian^{1,5}
8
9

10 ¹Department of Chemical and Environmental Engineering, University of Arizona, Tucson, AZ,
11 USA

12 ²Manila Observatory, Loyola Heights, Quezon City 1108, Philippines

13 ³Department of Physics, School of Science and Engineering, Ateneo de Manila University,
14 Loyola Heights, Quezon City 1108, Philippines

15 ⁴Institute of Environmental Science and Meteorology, University of the Philippines, Diliman,
16 Quezon City 1101, Philippines

17 ⁵Department of Hydrology and Atmospheric Sciences, University of Arizona, Tucson, AZ, USA
18

19 Correspondence to: Armin Sorooshian (armin@email.arizona.edu)

20 **Abstract**

21 This study analyzes mechanisms of long-range transport of aerosol and aerosol chemical
22 characteristics in and around East and Southeast Asia. Ground-based size-resolved aerosol
23 measurements collected at the Manila Observatory in Metro Manila, Philippines from July -
24 October 2018 were used to identify and contrast high and low aerosol loading events. Multiple
25 data sources, including models, remote-sensing, and in situ measurements, are used to analyze
26 the impacts of long-range aerosol transport on Metro Manila and the conditions at the local and
27 synoptic scales facilitating this transport. Through the use of case studies, evidence of long-range
28 transport of biomass burning aerosol and continental emissions is identified in Metro Manila.
29 Long-range transport of biomass burning aerosol from the Maritime Continent, bolstered by
30 southwesterly flow and permitted by low rainfall, was identified through model results and the
31 presence of biomass burning tracers (e.g. K, Rb) in the ground-based measurements. The
32 impacts of emissions transported from continental East Asia on the aerosol characteristics in
33 Metro Manila are also identified; for one of the events analyzed, this transport was facilitated by
34 the nearby passage of a typhoon. Changes in the aerosol size distributions, water-soluble
35 chemical composition, and contributions of various organic aerosol species to the total water-
36 soluble organic aerosol were examined for the different cases. The events impacted by biomass
37 burning transport had the overall highest concentration of water-soluble organic acids, while the
38 events impacted by long-range transport from continental East Asia, showed high percent
39 contributions from shorter chain dicarboxylic acids (i.e. oxalate) that are often representative of
40 photochemical and aqueous processing in the atmosphere. The low aerosol loading event was
41 subject to a larger precipitation accumulation than the high aerosol events, indicative of wet
42 scavenging as an aerosol sink in the study region. This low aerosol event was characterized by a
43 larger relative contribution from supermicrometer aerosols and had a higher percent contribution
44 from longer-chain dicarboxylic acids (i.e. maleate) to the water-soluble organic aerosol fraction,
45 indicating the importance of both primary aerosol emissions and local emissions. Results of this
46 study have implications for better understanding of the transport and chemical characteristics of
47 aerosol in a highly-populated region that has thus far been difficult to measure through remote-
48 sensing methods. Furthermore, findings associated with the effects of air mass mixing on aerosol
49 physiochemical properties are applicable to other global regions impacted by both natural and
50 anthropogenic sources.

51 **1. Introduction**

52 Better understanding of long-range transport of aerosol is critical for determining the fate
53 of atmospheric emissions and improving models of atmospheric aerosol. Nutrients (e.g. Duce et
54 al., 1991; Artaxo et al., 1994), bacteria (e.g. Bovallius et al., 1978; Maki et al., 2019), and
55 pollutants (e.g. Nordø, 1976; Lyons et al., 1978; Lindqvist et al., 1991) can be transported
56 through the atmosphere over large distances across the globe. Atmospheric aerosol can undergo
57 physiochemical changes through photochemical and aqueous-processing mechanisms such that
58 their characteristics at the emission source can be quite different from those farther downwind
59 (e.g. Yokelson et al., 2009; Akagi et al., 2012). Large uncertainties remain in atmospheric
60 aerosol models due to impacts of aqueous processing and wet scavenging on aerosol (Kristiansen
61 et al., 2016; Xu et al., 2019). Although impacts and processes of long-range aerosol transport
62 have worldwide applicability, the variety of meteorological conditions and emission sources that
63 can contribute to aerosol transport necessitate detailed analyses of transport events at the regional
64 level.

65 The plethora of both natural and anthropogenic emissions in and around the Southeast
66 (SE) Asia, the proximity of islands and continental regions in SE and East Asia, and the large,
67 growing population makes SE Asia a prime candidate for the study of long-range transport of
68 atmospheric aerosol. Moreover, the extensive cloud coverage and precipitation during certain
69 times of the year in SE Asia allow for an examination of the effects of aqueous processing and
70 wet scavenging. Characterizations of aerosol in mainland SE Asia and the Maritime Continent
71 (MC), which includes the islands south of the Philippines and north of Australia (e.g. islands part
72 of Malaysia and Indonesia), have found major emission sources to be industrial activities,
73 shipping, urban mega-cities, and biomass burning (Reid et al., 2013). In addition, natural
74 emission sources, including marine emissions, plant life, and occasionally volcanic eruptions,
75 intermingle with anthropogenic emissions. Mixing of aerosol from anthropogenic and biogenic
76 sources has been noted to be influential in the overall production of secondarily produced aerosol
77 via gas-to-particle conversion processes (Weber et al., 2007; Goldstein et al., 2009; Brito et al.,
78 2018). In addition, the mixing of marine and biomass burning emissions can produce
79 compositional changes, such as enhancements in chloride depletion (e.g. Braun et al., 2017) and
80 methanesulfonate (MSA) production (Sorooshian et al., 2015). The mechanisms governing
81 aerosol changes in mixed air masses have wide-ranging and complex impacts and require further
82 study in regions, such as SE Asia, that are impacted by multiple aerosol emission sources.

83 One major contributor to atmospheric aerosol in SE Asia and the MC that has received
84 considerable attention is biomass burning. Biomass burning in SE Asia appears to be dominated
85 by anthropogenic activities, such as peatland burning (Graf et al., 2009; Reid et al., 2013; Latif et
86 al., 2018) and rice straw open field burning (Gadde et al., 2009). However, current satellite
87 retrievals underestimate the true emissions in the region (Reid et al., 2013). Identification of
88 biomass burning emissions in the MC using satellite-based observations is difficult for numerous
89 reasons, including the characteristics of fires common to the region (e.g. low-temperature peat-
90 burning) and abundant cloud cover (Reid et al., 2012, 2013). However, the potential for long-
91 range transport of biomass burning emissions from the MC has received considerable attention
92 (Wang et al., 2013; Xian et al., 2013; Reid et al., 2016a; Atwood et al., 2017; Ge et al., 2017;
93 Song et al., 2018). In order to better understand the frequency, amount, and fate of biomass
94 burning emissions in the MC and SE Asia, both in situ measurements and modeling studies are
95 needed. Insights into the fate of biomass burning emissions in the atmosphere are crucial and

96 applicable on a global scale, especially since studies have indicated an increasing trend in
97 biomass burning worldwide (Flannigan et al., 2009, 2013).

98 As a mega-city in SE Asia, Metro Manila, Philippines (Population ~12.88 million;
99 Philippine Statistics Authority, 2015) is a prime location for the study of locally-produced urban
100 anthropogenic aerosol (Kim Oanh et al., 2006) that is mixed with biogenic, natural, and
101 anthropogenic pollutants from upwind areas. Previous research conducted at the Manila
102 Observatory (MO) in Quezon City, Metro Manila characterized PM_{2.5} (particulate matter (PM)
103 with aerodynamic diameter less than 2.5 μm) and sources of measured particles, with traffic
104 emissions being the major source at MO (Simpas et al., 2014). Interestingly, levels of measured
105 PM_{2.5} at MO showed little variance between the wet (June-October) and dry seasons (Simpas et
106 al., 2014). Additional studies have further characterized vehicular emissions by focusing on
107 black carbon (BC) particulate concentrations in sites around the Metro Manila region, including
108 near roadways (Bautista et al., 2014; Kecorius et al., 2017; Alas et al., 2018). Due to very high
109 population density in Metro Manila, it is expected that many of the urban PM sampling sites are
110 highly affected by local anthropogenic sources as opposed to long-range transport. However, the
111 proximity of the Philippines to other islands and continental Asia raises the question of the
112 relative impacts of long-range transport as opposed to local emissions on not just Metro Manila,
113 but also downwind regions.

114 Long-range transport to the Philippines varies by season since there is a strong change in
115 weather patterns throughout the year (Bagtasa et al., 2018). Another study of the aerosol over the
116 South China Sea (SCS), which is bordered to the east by the Philippines, found seasonal changes
117 in aerosol emission sources, with year-round anthropogenic pollution, smoke from the MC
118 between August – October, and dust from northern continental Asia between February – April
119 (Lin et al., 2007). The season from approximately June – September (Cayanan et al., 2011; Cruz
120 et al., 2013), referred to as the Southwest Monsoon (SWM) season, is characterized by increased
121 prevalence of southwesterly winds and precipitation. During the SWM season, biomass burning
122 is prevalent in the MC, while biomass burning is more common in continental SE Asia during
123 the winter and spring (Lin et al., 2009; Reid et al., 2013). While variability exists in the start dates
124 of the different seasons, the northeast monsoon transition generally occurs in October (Cruz et
125 al., 2013), and previous research has defined this season as occurring from October – February
126 (Bagtasa, 2011). During the northeast monsoon, aerosol influences from northern East Asia were
127 measured in the northwestern edge of the Philippines (Bagtasa et al., 2018). In addition to
128 transport of aerosol to the Philippines, the influence of emission outflows from the Philippines
129 has also been measured in the northern SCS at Dongsha Island (Chuang et al., 2013) and in
130 coastal southeast China (Zhang et al., 2012). Long-range transported aerosol in SE and East Asia
131 have various sources, and therefore, different physiochemical properties. However, the
132 prevalence of the signal of long-range transported aerosol in a highly polluted mega-city, such as
133 Metro Manila, is not well characterized.

134 As recent studies have indicated a decline in SWM rainfall in the western Philippines and
135 an increase in no-rain days during the typical SWM season (Cruz et al., 2013), the potential for
136 wet scavenging of aerosol during these time periods could be decreasing. Furthermore, decreases
137 in monsoonal rainfall in other parts of Asia, including India (Dave et al., 2017) and China (Liu et
138 al., 2019), have been linked to increases in aerosol, especially those of anthropogenic origin.
139 Reinforcing mechanisms in these interactions, such as decreased rainfall reducing wet
140 scavenging, leading to higher aerosol concentrations that in turn suppress precipitation, and the
141 corresponding climatic changes in monsoonal rain in the western Philippines underscore the need

142 to better understand the processes governing atmospheric aerosol characteristics and sources,
143 especially during the monsoonal season.

144 The present study focuses on three high-aerosol loading events, contrasted with a very
145 low aerosol event, as identified by ground-based observations collected at MO from July -
146 October 2018. The objectives of the study are to (i) describe synoptic and local scale conditions
147 facilitating various transport cases, (ii) characterize aerosol physicochemical properties
148 associated with long-range transport, and (iii) identify transformational processes, especially
149 with regard to chemical composition, of aerosol during long-range transport to the highly-
150 populated Metro Manila region. The results of this work have implications for better
151 understanding of (i) the fate of biomass burning emissions in a region with prevalent wildfires
152 that are poorly characterized by remote-sensing, (ii) the impact of transformational and removal
153 mechanisms, including aqueous processing, photochemical reactions, and wet scavenging, on
154 long-range transported aerosol from multiple sources, and (iii) typical synoptic and local scale
155 behavior of aerosol in a region that is both highly populated and gaining increasing attention due
156 to campaigns such as the NASA-sponsored Clouds, Aerosols, and Monsoon Processes
157 Philippines Experiment (CAMP²Ex).
158

159 **2. Methodology**

160 **2.1 Ground-Based Observations**

161 As part of a year-long sampling campaign (CAMP²Ex weathER and CompoSition
162 Monitoring: CHECSM) at the Manila Observatory (MO; 14.64° N, 121.08° E) in Quezon City,
163 Metro Manila, Philippines, 12 sets of size-resolved aerosol were collected from July - October
164 2018 using a Micro-Orifice Uniform Deposit Impactor (MOUDI; Marple et al., 2014). Details
165 for the 12 size-resolved sets can be found in Table 1. Sample Teflon substrates (PTFE
166 membrane, 2 μm pore, 46.2 mm diameter, Whatman) were cut in half for preservation for future
167 analysis. Half-substrates were extracted in 8 mL of Milli-Q water (18.2 MΩ-cm) in sealed
168 polypropylene vials through sonication for 30 min. Aqueous extracts were subsequently analyzed
169 for ions using ion chromatography (IC; Thermo Scientific Dionex ICS-2100 system) and
170 elements using triple quadrupole inductively coupled plasma mass spectrometry (ICP-QQQ;
171 Agilent 8800 Series). The list of analyzed species and limits of detection for those species can be
172 found in Table S1, with limits of detection in the ppt range for ICP and the ppb range for IC.
173 Background concentrations were also subtracted from each sample. For each MOUDI set
174 (naming convention: MO#), the mass concentration sum of the water-soluble species was
175 calculated; using this summation, the three high-aerosol loading events were identified (MO7,
176 MO12, and MO14), as well as the lowest aerosol event (MO11). The average ± standard
177 deviation of the total-water soluble species measured for the remaining 8 sets not identified in
178 the high or low categories is $6.99 \pm 2.71 \mu\text{g m}^{-3}$.
179

180 **2.2 Remote-Sensing Observations**

181 Retrievals of atmospheric profiles from the Cloud-Aerosol Lidar with Orthogonal
182 Polarization (CALIOP) onboard the Cloud-Aerosol Lidar and Infrared Pathfinder Satellite
183 Observations (CALIPSO) were taken for select satellite overpasses corresponding to MOUDI
184 sample sets of interest (Winker et al., 2009). Previous studies have examined the ability of
185 CALIOP to capture atmospheric profiles in SE Asia and the MC, with one major challenge in
186 this region being the lack of cloud-free schemes (Campbell et al., 2013; Ross et al., 2018).
187 Overpasses corresponding to the three highest aerosol events were analyzed, but no data was

188 available for the time encompassing MO11. The CALIOP Level 2 Vertical Feature Mask (VFM)
189 Version 4.20 was used to distinguish between clear air, clouds, and aerosol (Vaughan et al.,
190 2004). For figures of CALIOP VFM data in this study, data are plotted at 30 m vertical
191 resolution every 5 km along the satellite ground-track.

192

193 **2.3 Models**

194 To describe the synoptic scale conditions, data were used from the Modern-Era
195 Retrospective analysis for Research and Applications, Version 2 (MERRA-2; Gelaro et al.,
196 2017). Horizontal winds at 850 hPa (GMAO, 2015a) were temporally averaged over the
197 sampling period using 3-hourly instantaneous data and subsequently spatially averaged to
198 increase figure readability. The total cloud area fraction (GMAO, 2015b) was also temporally
199 averaged over the sampling period using 1-hourly time-averaged MERRA-2 data.

200 Five-day air mass back-trajectories were calculated using the Hybrid Single Particle
201 Lagrangian Integrated Trajectory (HYSPLIT) model from NOAA (Stein et al., 2015) and
202 gridded meteorological data from the National Centers for Environmental Prediction/National
203 Center for Atmospheric Research (NCEP/NCAR) reanalysis project. The model was run for
204 back-trajectories terminating at the MOUDI inlet (~85 m above sea level) starting at the
205 beginning of the sample set and every 6 h thereafter during each sample set, resulting in $(1 +$
206 $N/6)$ trajectories for each set, where N is the total number of sampling hours. The HYSPLIT
207 model has been used extensively in studies focused on regions across the globe to study aerosol
208 transport (Stein et al., 2015).

209 Precipitation amounts were found using the Precipitation Estimation from Remotely
210 Sensed Information using Artificial Neural Networks—Cloud Classification System
211 (PERSIANN-CCS) dataset (Hong et al., 2004), which is available from the UC Irvine Center for
212 Hydrometeorology and Remote Sensing (CHRS) Data Portal (<http://chrsdata.eng.uci.edu>,
213 Nguyen et al., 2019). PERSIANN-CCS has previously been used to analyze precipitation events
214 in the region of interest, as shown by the successful characterization of rainfall during Typhoon
215 Haiyan over the Philippines in November 2013 (Nguyen et al., 2014). Benefits of PERSIANN-
216 CCS include the data availability at $0.04^\circ \times 0.04^\circ$ spatial resolution, while uncertainties in the
217 dataset arise from sources such as a lack of bias correction (Nguyen et al., 2014). Precipitation
218 accumulated during the sample sets (Table 1) was calculated to be the average found for the
219 region surrounding MO in the box bounded by $121.0199 - 121.0968^\circ$ E and $14.6067 - 14.6946^\circ$
220 N.

221 To further describe long-range transport activity, results from the Navy Aerosol Analysis
222 and Prediction System (NAAPS) operational model are included for the selected study periods
223 (Lynch et al., 2016; <https://www.nrlmry.navy.mil/aerosol/>). Global meteorological fields used in the
224 NAAPS model are supplied by the Navy Global Environmental Model (NAVEM; Hogan et al.,
225 2014). The NAAPS model has previously been employed to study aerosol in the MC (e.g. Xian
226 et al., 2013).

227

228 **3. Results**

229 **3.1 Cases of Long-Range Aerosol Transport**

230 The following sub-sections (3.1.1-3.1.4) describe the synoptic and local scale
231 meteorological conditions governing long-range aerosol transport during the three highest
232 aerosol events (MO7, MO12, and MO14) and, for the purposes of comparison, the lowest aerosol

233 event (MO11). Also included are characterizations of aerosol from remote-sensing and model
234 results. Results of size-resolved aerosol characterization at MO are discussed in Section 3.2.

235

236 **3.1.1 MO7 (August 14 – 16, 2018): Smoke Transport from Maritime Continent**

237 Many previous studies have focused on the prevalence of biomass burning in the MC and
238 the potential for transport of smoke towards the Philippines (Wang et al., 2013; Xian et al., 2013;
239 Reid et al., 2016a; Atwood et al., 2017; Ge et al., 2017; Song et al., 2018). Figure 1a shows the
240 average 850 hPa wind vectors and cloud fraction for the MO7 sampling period. The prevailing
241 wind direction was towards the northeast, consistent with typical SWM flow. Furthermore, areas
242 with lower cloud coverage were present to the southwest of Metro Manila. The HYSPLIT back-
243 trajectory for this sample set also shows an air mass originating around the MC to the southwest
244 of MO that is then transported over the ocean towards the Philippines (Figure 2a). As evidenced
245 by the name of the season (i.e. Southwest Monsoon), this trajectory is typical for this time of the
246 year and was the dominating trajectory pattern for the remaining eight sample sets not chosen for
247 in-depth analysis (Figure S1). Furthermore, for MO1 – MO10 (i.e. all sample sets with prevailing
248 southwesterly wind influence), MO7 had the lowest rain amount for the surrounding region,
249 followed by MO8, which had the 4th highest water-soluble aerosol concentration (Table 1). This
250 suggests that wet scavenging could have been less influential in MO7 and MO8, thereby leading
251 to an increase in the PM measured. Three CALIPSO overpasses near MO occurred during the
252 MO7 sample set and one occurred during the nighttime after sampling ended; however, the
253 signal was largely attenuated in the lower 8 km during the daytime samples for the area
254 surrounding MO (Figure S2). In the case of the two nighttime overpasses (Figure 3), which
255 sampled to the southwest of Manila, a deep aerosol layer is observed in the VFM extending from
256 the surface to around 3 km (Figure 3). This classic case of long-range transport from the MC to
257 the Philippines during the SWM season is also clearly shown in the biomass burning smoke
258 surface concentrations from the NAAPS model (Figure 4a).

259

260 **3.1.2 MO11 (September 18 – 20, 2018): Lowest Aerosol Event**

261 MO11 had the lowest overall water-soluble aerosol mass concentration ($2.7 \mu\text{g m}^{-3}$),
262 which is over six times lower than the highest aerosol MOUDI set. As evidenced by both the 850
263 hPa wind vectors (Figure 1b) and the HYSPLIT back-trajectories (Figure 2b) from this set,
264 conditions are very different from the highest three aerosol events and show transport patterns
265 with flow originating over the open ocean to the east of the Philippines moving almost due west.
266 The lack of anthropogenic aerosol sources in the path of the back-trajectories could result in the
267 overall low amount of aerosol observed. This set was also characterized by high accumulated
268 rainfall amounts for the region in the path of the back-trajectories (Figure 2b) and in the area
269 surrounding MO as compared to the highest aerosol events (Table 1), increasing the possibility
270 that wet scavenging effectively removed most of the transported (and, to some extent, local)
271 aerosol. In addition, the NAAPS model showed no smoke influence from the MC and an isolated
272 anthropogenic and biogenic fine aerosol plume around Metro Manila, suggesting local sources
273 accounted for the majority of the measured aerosol (Figure 4b).

274

275 **3.1.3 MO12 (September 26 – 28, 2018): Impacts of Typhoon Trami**

276 Typhoon Trami (Category 5) passed to the northeast of the island of Luzon in the
277 Philippines during MO12 (Figure 1c). Typhoon influences on atmospheric aerosol, caused by
278 varying factors such as wind speed and precipitation, have been studied in China (Yan et al.,

279 2016; Liu et al., 2018), Korea (Kim et al., 2007), Malaysia (Juneng et al., 2011), the South China
280 Sea (Reid et al., 2015, 2016b), and Taiwan (Fang et al., 2009; Chang et al., 2011; Lu et al.,
281 2017). The influences of typhoons on biomass burning emissions and transport in the MC have
282 also been examined (Reid et al., 2012; Wang et al., 2013). In this case, the influence of this storm
283 changed the prevailing wind direction approaching the northern Philippines, effectively pulling
284 an air mass from the west of the island, and along with it, emissions from continental East Asia
285 (Figure 2c). Furthermore, the air mass passed through regions of relatively little rainfall during
286 transport to the Philippines (Figure 2c), and accumulated rainfall at MO during this sample set
287 was very low (Table 1). One CALIPSO overpass around the ending time of set MO12 and one
288 during the nighttime after sampling ended (Figure 3) show that in the direction of transport (i.e.
289 north of the MO, from around 15-20° N), there is an aerosol layer extending up to around 2 km
290 during the day (northwest of MO) and 3 km at night (northeast of MO). The influence of
291 emissions from continental East Asia is also apparent in the NAAPS model (Figure 4c).
292 Observations at Dongsha Island, located to the north of the Philippines, have revealed influence
293 from Gobi Desert emissions (Wang et al., 2011) and anthropogenic sources (Atwood et al.,
294 2013). Farther south in the MC, aerosol measurements in Malaysia have also indicated influence
295 of aged, long-range transport from sites to the north in East Asia (Farren et al., 2019).

296

297 **3.1.4 MO14 (October 6 – 8, 2018): Mixed Influences**

298 The final MOUDI set (MO14) included in this study represents a transition in
299 meteorological regimes at the end of the SWM season and resulted in the highest overall water-
300 soluble mass concentration. This event had some of the lowest rainfall amounts in the region
301 surrounding Metro Manila (Figure 2d), with zero accumulated precipitation at MO during the
302 sampling period (Table 1). Furthermore, low cloud fraction was observed for regions to the
303 northwest and east of Metro Manila (Figure 1d). Back-trajectories from HYSPLIT show that the
304 air mass appeared to be influenced by a mix of continental sources in East Asia and local sources
305 (Figure 2d). Furthermore, two CALIPSO overpasses, one during the nighttime while sampling
306 was occurring and the other during the daytime after sampling ended, show a deep aerosol layer
307 north of MO, extending from the surface to around 2 km on October 6th and lower on October 8th
308 (Figure 3). From the NAAPS model, it appears that a mixture of MC smoke emissions and
309 continental East Asia emissions converge around the northern Philippines (Figure 4d).

310

311 **3.2. Ground-Based Aerosol Chemical Composition**

312 **3.2.1 Size-Resolved Aerosol Characteristics**

313 The water-soluble mass size distributions and the percent contribution of each MOUDI
314 stage to the water-soluble mass for the four sets of interest (MO7, MO12, MO14, and MO11)
315 and the average (\pm one standard deviation) of the remaining sets (MO1 – MO6, MO8 – MO10)
316 are shown in Figure 5. Most of the sets show a bimodal distribution with peaks in both the
317 submicrometer and supermicrometer range; one exception is the lowest aerosol event (MO11),
318 which shows a fairly broad size distribution. The highest aerosol event, MO14, shows a
319 significant peak in the submicrometer range, with a very large drop in mass concentration in the
320 supermicrometer range. This is in stark contrast to the lowest aerosol event (MO11), which
321 shows that the supermicrometer range contributes the greatest percent to the total water-soluble
322 mass. The second and third highest aerosol events, MO7 and MO12, also show significant
323 enhancements in the supermicrometer range as compared to the average of the other sets and
324 MO14.

325 Examination of the major species contributing to the water-soluble mass (Figure 6) can
326 lend additional insights into the variability in the size distributions. MO14 had one of the highest
327 combined contributions of SO_4^{2-} and NH_4^+ (77.2% of water-soluble mass), with only MO10
328 being slightly larger at 77.6%. These two species are typically associated with the submicrometer
329 range and anthropogenic origins due to their formation through secondary processes such as gas-
330 to-particle conversion of gaseous SO_2 and NH_3 , respectively, and aqueous processing to form
331 SO_4^{2-} (Ervens, 2015). In contrast, MO11 had the lowest overall combined percent contribution of
332 these two species (41.4%) to the water-soluble aerosol mass. Of all 12 SWM MOUDI sets,
333 MO11 had the highest percent contributions from Ca^{2+} (14.0%) and Cl^- (12.5%), as well as one
334 of the highest contributions from Na^+ (10.7%). Each of these species is associated with primary
335 emissions, including dust in the case of Ca^{2+} and sea salt for Na^+ and Cl^- , resulting in larger
336 particles (i.e. $> 1 \mu\text{m}$). The HYSPLIT back-trajectories for MO11 match well with the MOUDI
337 results, as the influence of marine aerosol (i.e. Na^+ , Cl^-) and lack of anthropogenic sources of
338 SO_2 and NH_3 is apparent. Local sources of dust most likely contribute the highest amount to the
339 measured Ca^{2+} , as the back-trajectories show few other crustal sources farther upwind. Average
340 size-resolved profiles for all of the species in these 12 sample sets can be found in Cruz et al.
341 (2019), with characteristic size distribution profiles agreeing with the above assessments.
342

343 3.2.2 Enhancements in Tracer Species

344 In addition to insights from the major water-soluble chemical species found in aerosol,
345 tracer aerosol species can also be used to identify impacting emission sources (e.g. Fung and
346 Wong, 1995; Allen et al., 2001; Ma et al., 2019). For the aforementioned high aerosol events,
347 numerous tracer species are elevated in some, but not all, sample sets. This makes these species
348 prime candidates for linking influencing sources to the measured ambient aerosol. The authors
349 theorize that MO8, which was the 4th highest aerosol event (Table 1), also was impacted by
350 biomass burning due to the back-trajectory analysis (Figure S1), NAAPS model (Figure S3), and
351 increases in select species described subsequently. Therefore, MO8 was separated from the other
352 sample sets for the purposes of the following characterizations. Figure 7 shows the size-resolved
353 aerosol composition for select tracer species for the four highest aerosol events (MO7, MO8,
354 MO12, and MO14), the lowest aerosol event (MO11), and the average (\pm standard deviation) of
355 the remaining seven sample sets.

356 Potassium is frequently used as a biomass burning tracer (e.g. Andreae, 1983; Artaxo et
357 al., 1994; Echalar et al., 1995; Chow et al., 2004; Thepnuan et al., 2019). This species shows
358 highly elevated levels in the submicrometer range for MO7 and MO8 (i.e. the sets influenced by
359 biomass burning transport from the MC). Other elevated trace elements for these two profiles
360 include Rb, Cs, Se, and Ti (Figure 7). Previous studies in the western United States (Schlosser et
361 al., 2017; Ma et al., 2019) have also shown Rb enhancements in wildfire-influenced aerosol. Rb
362 has also been measured in flaming and smoldering biomass burning emissions (Yamasoe et al.,
363 2000). Enhancements in Rb and Cs in the fine fraction of aerosol influenced by wildfire
364 emissions have been observed in South Africa (Maenhaut et al., 1996), with similar results
365 shown in this study for aerosol in the submicrometer size range. Se is also enhanced for these
366 two sets in the submicrometer range, as it is often formed through gas-to-particle conversion
367 processes of inorganic Se compounds (Wen and Carignan, 2007). A wide variety of sources for
368 atmospheric Se exist (Mosher and Duce, 1987), including, but not limited to, coal combustion
369 (Thurston and Spengler, 1985; Fung and Wong, 1995; Song et al., 2001), marine emissions
370 (Arimoto et al., 1995), volcanos, and biomass burning (Mosher and Duce, 1987). In contrast to

371 the other enhanced species for MO7 and MO8, the mass concentration mode for Ti resides in
372 supermicrometer size range. Ti is typically associated with crustal material that can be suspended
373 through mechanisms such as vehicle usage (Sternbeck et al., 2002; Querol et al., 2008; Amato et
374 al., 2009) and lofting in wildfire plumes (Maudlin et al., 2015; Schlosser et al., 2017). While
375 long-range transport of biomass burning aerosol could lead to the enhancements measured for
376 these biomass burning tracer species, local emission sources, such as waste burning and wood
377 burning for cooking, may also play a role.

378 Two tracer species are included that showed enhancements for MO12, specifically Ba in
379 the supermicrometer range and V in the submicrometer range (Figure 7). One well-documented
380 source of aerosol Ba is non-exhaust vehicle emissions, including brakewear (Sternbeck et al.,
381 2002; Querol et al., 2008; Amato et al., 2009; Jeong et al., 2019). V also has well characterized
382 emission sources, most specifically fuel combustion (Fung and Wong, 1995; Artaxo et al., 1999;
383 Song et al., 2001; Lin et al., 2005; Kim and Hopke, 2008). In coastal environments, V is often
384 tied to shipping emissions (Agrawal et al., 2008; Pandolfi et al., 2011; Maudlin et al., 2015;
385 Mamoudou et al., 2018). As these sources are anthropogenic in origin, it is difficult to determine
386 the relative influences of long-range transport versus local emissions, especially with the
387 proximity of the sampling site to major roadways and shipping in Manila Bay. However, the
388 enhancement in V could result from the transport of the aerosol over major shipping lanes father
389 upwind.

390 Finally, Figure 7 shows three selected elements that appear enhanced in MO14, all of
391 which are typically tied to anthropogenic sources. Both Pb and Sn are found mainly in the
392 submicrometer range and have been linked by previous studies to vehicle emissions (Singh et al.,
393 2002; Amato et al., 2009), industrial emissions (Querol et al., 2008; Allen et al., 2001), and
394 waste burning (Kumar et al., 2015). Other sources of Pb could include E-waste recycling
395 (Fujimori et al., 2012) and biomass burning (Maenhaut et al., 1996). The size distribution of Mo
396 for MO14 shows a much broader distribution, with peaks in both the sub- and supermicrometer
397 ranges. Sources of Mo include vehicle emissions (Pakkanen et al., 2003; Amato et al., 2009),
398 combustion (Pakkanen et al., 2001, 2003), and industrial activity, including copper smelters
399 (Artaxo et al., 1999). As is the case with the enhanced species in MO12, the anthropogenic
400 nature of these species makes it difficult to determine the relative contribution of long-range
401 versus local emissions. However, as both MO12 and MO14 show enhancements in
402 anthropogenic-produced trace elements, the influence of long-range transport from industrial and
403 urban areas in continental East Asia is plausible.

404

405 **3.2.3 Variability of Water-Soluble Organic Species**

406 Water-soluble organic aerosol species serve as good tracers for emission sources, impact
407 the cloud condensation nuclei (CCN) budget, and contribute non-negligible mass to atmospheric
408 aerosol. Figure 8 shows the sum of the total measured water-soluble organic species and the
409 relative contributions of oxalate, succinate, adipate, maleate, pyruvate, MSA, and phthalate to the
410 total measured water-soluble organics for MO7, MO8, MO11, MO12, MO14, and the average (\pm
411 one standard deviation) of the remaining sets. Malonate (C3) was not characterized due to its low
412 concentrations in the samples measured and the co-elution of C3 with carbonate in the IC
413 analysis. Glutarate (C5) was also excluded from the analysis due to very low concentrations. For
414 the examination of the organic species, MO8 was again separated from the other MOUDI sets
415 due to it having the second highest concentration of organic species ($0.66 \mu\text{g m}^{-3}$) and an organic
416 species contribution profile very similar to that of MO7. The remaining MOUDI sets included in

417 the average category (MO1 – MO6, MO9 – MO10) all have total organic species concentrations
418 that were less than the four highest aerosol sets (MO7, MO8, MO12, MO14) and greater than the
419 lowest aerosol set (MO11). The lowest aerosol event (MO11) has the lowest overall
420 concentration of organic aerosol ($0.09 \mu\text{g m}^{-3}$), while the 2nd highest aerosol event (MO7) has the
421 highest concentration of organic aerosol ($0.70 \mu\text{g m}^{-3}$).

422 Many studies worldwide have examined the relative contributions of organic species to
423 atmospheric aerosol, with oxalate typically having the highest contribution among dicarboxylic
424 acids (Kawamura and Kaplan, 1987; Kawamura and Ikushima, 1993; Kawamura and Sakaguchi,
425 1999; Sorooshian et al., 2007a; Hsieh et al., 2007, 2008; Aggarwal and Kawamura, 2008;
426 Deshmukh et al., 2012, 2018; Li et al., 2015; Hoque et al., 2017; Kunwar et al., 2019). Oxalate
427 was the dominant water-soluble organic species for all 12 MOUDI sets, with oxalate having the
428 highest contribution to the organic aerosol in MO12 (88.7% of total organic aerosol). Oxalate is
429 often considered a byproduct of photochemical aging of longer-chain dicarboxylic acids (e.g.
430 Kawamura and Ikushima, 1993; Kawamura and Sakaguchi, 1999), and therefore an increase in
431 oxalate is often considered a signature of aged aerosol in the absence of primary oxalate
432 emissions from sources such as biomass burning. Another major pathway of oxalate formation is
433 aqueous processing (Crahan et al., 2004; Ervens et al., 2004, 2018; Sorooshian et al., 2006,
434 2007b; Wonaschuetz et al., 2012), which is likely prevalent during the SWM when there is
435 frequent cloud cover. Previous studies have also demonstrated the ability for transport of and
436 photochemical aging of water-soluble organic acids over long distances in a marine environment
437 (e.g. Kawamura and Sakaguchi, 1999) and the importance of emissions from continental Asia in
438 the organic aerosol budget in the western north Pacific (Aggarwal and Kawamura, 2008; Hoque
439 et al., 2017). The back-trajectories of the air masses terminating at MO during MO12 and MO14
440 indicate origins of emissions from continental East Asia (Figure 2). It is plausible that the high
441 contribution of oxalate to the organic aerosol in MO12 and MO14 (which had the fourth highest
442 percent contribution of oxalate) is due to the degradation of both primarily-emitted and
443 secondarily-produced longer-chain dicarboxylic acids during the transport process through
444 mechanisms described above, such as photochemical degradation and aqueous processing, with
445 the former mechanism being plausible in the regions of low cloud cover to the north and
446 northwest of the Manila (Figure 1) and the latter mechanism potentially being of great
447 importance due to the typhoon influences during transport. While the aerosol measured in MO7
448 and MO8 also show long-range transport influences (Figure 2a and Figure S1), the overall signal
449 of organic aerosol is much stronger in these two sets, such that the absolute concentration of
450 oxalate (MO7: $0.47 \mu\text{g m}^{-3}$ and MO8: $0.42 \mu\text{g m}^{-3}$) is still greater than in MO12 ($0.19 \mu\text{g m}^{-3}$)
451 and MO14 ($0.37 \mu\text{g m}^{-3}$). However, biomass burning is a well-documented source of both
452 oxalate and longer-chain dicarboxylic acids (e.g. Falkovich et al., 2005; Nirmalkar et al., 2015;
453 Cheng et al., 2017; Deshmukh et al., 2018; Thepnuan et al., 2019).

454 Succinate has been linked to biomass burning emissions (Wang and Shooter, 2004;
455 Falkovich et al., 2005; Zhao et al., 2014; Balla et al., 2018), vehicular emissions (Kawamura and
456 Kaplan, 1987; Kawamura et al., 1996; Yao et al., 2004), and secondary production via
457 photochemical reactions of precursor organic compounds (Kawamura and Ikushima, 1993;
458 Kawamura et al., 1996; Kawamura and Sakaguchi, 1999). The two MO MOUDI sets thought to
459 have the most influence from biomass burning emissions (MO7 and MO8) had the highest
460 organic aerosol mass concentrations and the highest mass percent contributions of succinate to
461 the organic aerosol (MO7: 14.3% and MO8: 17.5%). In contrast, the next highest contribution of
462 succinate to the organic aerosol was 4.2% measured in MO5. These results agree with previous

463 studies in Northeast China that showed an increase in total organic aerosol mass concentration
464 and a strong increase (decrease) in the relative contribution of succinate (oxalate) during biomass
465 burning periods as opposed to non-biomass burning periods (Cao et al., 2017). Results from
466 California, USA also showed higher percent contributions of succinate to the water-soluble
467 organic aerosol during periods influenced by biomass burning (Maudlin et al., 2015).

468 MO11 had the second highest relative contribution of maleate (28.5% of water-soluble
469 organic aerosol) out of all 12 sample sets and had a much higher percent contribution as
470 compared to the four highest aerosol events (<2.5% for each of the following: MO7, MO8,
471 MO12, and MO14). Maleate is linked to the oxidation of aromatic hydrocarbons, usually from
472 anthropogenic sources such as vehicular emissions (Kawamura and Kaplan, 1987; Kunwar et al.,
473 2019). One explanation for this result could be the higher rainfall accumulation in and around the
474 study region during MO11 as compared to the three highest aerosol sets (Figure 2). Wet
475 scavenging could have removed aerosol from transported air masses during their journey towards
476 MO, thereby increasing the relative contribution of local sources to the measured aerosol in
477 MO11. Because of the reduced aging time associated with emissions from local sources, the
478 relative increase in the contribution of longer-chain dicarboxylic acids and the decrease in the
479 relative contribution of oxalate is plausible. Hsieh et al. (2008) showed in samples from Taiwan
480 that the relative contribution of oxalate to the organic acids was also higher during periods of
481 high aerosol loading as opposed to periods of moderate aerosol loading when the overall PM
482 concentration was lower. MO11, which showed air mass back-trajectories originating to the east
483 of the Philippines from the open Pacific (Figure 2b), had the lowest overall water-soluble PM
484 concentration, the lowest overall concentration of water-soluble organic acids, and the second
485 lowest percent contribution of oxalate to the organic acid mass (57.1%) of all the sets.

486 Phthalate is an aromatic dicarboxylic acid often linked to anthropogenic sources through
487 photochemical transformation of emissions from vehicles (Kawamura and Kaplan, 1987;
488 Kawamura and Ikushima, 1993) and waste burning (Kumar et al., 2015), although aqueous
489 processing has also been proposed as a formation mechanism (Kunwar et al., 2019).
490 Accordingly, phthalate has been shown to have seasonal and diurnal variations in concentration,
491 with enhanced production usually linked to times of stronger solar radiation (i.e. summertime
492 and daytime: Satsumabayashi et al., 1990; Ray and McDow, 2005; Ho et al., 2006; Kunwar et
493 al., 2019). However, increased emissions of precursor species during different times of the year
494 may affect these trends (Hyder et al., 2012). Sets MO7, MO8, MO11, and MO14 had the highest
495 contribution to the water-soluble organics from phthalate (range: 9.5 – 10.2%). In contrast, the
496 remaining sets had a much lower contribution (range: 1.7 – 4.9%). However, the absolute
497 concentration of phthalate was highest in sets MO7, MO8, and MO14 (range: 45.3 – 67.0 ng m⁻³),
498 and much lower for the remaining sets (range: 2.0 – 8.9 ng m⁻³). Increased phthalate
499 concentrations during biomass burning episodes have been previously measured in SE Asia (Cao
500 et al., 2017). Furthermore, cloud coverage was fairly low during MO14 as compared to the other
501 sets of interest (Figure 1), increasing the possibility of photochemical production of phthalate.
502 For the remaining sample sets, the range of phthalate concentrations is substantially lower and
503 fairly consistent, indicating that the measured phthalate in these samples most likely represents
504 the local background conditions.

505 While not a carboxylic acid, MSA is nonetheless an important organic aerosol species,
506 especially in marine environments. The assumed precursor of MSA in this study is from the
507 oxidation of marine-emitted dimethylsulfide (DMS). Interestingly, all sample sets showed
508 approximately the same mass percent contribution of MSA to the organic aerosol, ranging from a

509 minimum of 3.1% (MO6) to a maximum of 7.0% (MO5). However, the absolute concentration
510 of MSA was highest in the two sets with biomass burning influence (MO7: 23.3 ng m⁻³ and
511 MO8: 21.4 ng m⁻³), with concentrations 8.4 and 7.7 times higher, respectively, than the lowest
512 MSA concentration measured (MO11: 2.8 ng m⁻³). A previous study showed that MSA
513 concentrations in air masses with mixed influence from marine and biomass burning emissions
514 are higher than the concentrations measured from either source alone (Sorooshian et al., 2015).
515 The results from the present study (i.e. more MSA measured in sets with biomass burning
516 influence) in SE Asia again highlight the complexity of interactions between air masses with
517 different sources and the accompanying changes in aerosol physiochemical properties.
518

519 **4. Conclusions**

520 This study sought to characterize influences of local and long-range transported aerosol
521 to the Philippines during the Southwest Monsoon (SWM) season as well as the various synoptic
522 and local scale conditions that facilitate and suppress long-range transport of aerosol. As a highly
523 populated mega-city, Metro Manila is the source of a large amount of urban, anthropogenic
524 pollution. However, synoptic-scale weather, including the typical SWM flow and typhoons, can
525 impact the transport of aerosol to and from Metro Manila. While previous work in a rural area in
526 the northwest edge of the Philippines has identified seasonal aerosol transport patterns to the
527 Philippines using PM_{2.5} data (Bagtasa et al., 2018), the present study highlights case studies of in
528 situ size-resolved aerosol measurements from Metro Manila to examine the potential for aerosol
529 transport to impact this urban area as well.

530 For two of the sample sets with enhanced total water-soluble aerosol mass concentration,
531 biomass burning aerosol transport from the Maritime Continent (MC) towards the Philippines
532 was identified using air mass back-trajectories and the Navy Aerosol Analysis and Prediction
533 System (NAAPS) model. This transport followed a southwesterly flow pattern that is typical of
534 this time of year (Figure S1) and lends its name to the SWM season. Deep aerosol layers,
535 extending from the surface to 3 km, were identified by CALIOP to the southwest of the
536 Philippines. The influence on aerosol in Metro Manila was shown through enhancements in
537 biomass burning tracer species (e.g. K, Rb) and increased concentration of organic aerosol. The
538 challenges in satellite-based retrievals of biomass burning in the region (Reid et al., 2012, 2013)
539 and the underestimation of fire activity in the region by these satellite retrievals (Reid et al.,
540 2013) lead to unanswered questions about the amount and fate of biomass burning emissions in
541 the MC and SE Asia. The ability to measure biomass burning signatures in a highly polluted,
542 urban mega-city such as Metro Manila and the evidence of long-range transport gathered through
543 multiple methods and data sources (i.e. in situ measurements, models, and remote-sensing)
544 speaks to the strong signature of biomass burning emissions in the region and the long-range
545 transport pathways available for these emissions.

546 In contrast, transport of anthropogenic emissions from continental East Asia was
547 identified on two occasions with high water-soluble aerosol mass concentrations, with one
548 measured instance of long-range transport having been facilitated by the influence of a typhoon.
549 In these cases, it is difficult to separate urban emissions between local and distant sources.
550 However, the elevation of select tracer species (Ba, V, Pb, Mo, Sn) and the water-soluble organic
551 aerosol characteristics for these two cases (i.e. high relative contribution of oxalate to the organic
552 aerosol) indicated that long-range transported urban emissions could impact Metro Manila.

553 Finally, one low aerosol loading case was impacted by air masses travelling over the
554 open ocean to the east of the Philippines. This case showed an enhanced fraction of

555 supermicrometer aerosol and a very low concentration of water-soluble organic acids. Higher
556 rain accumulation during this sample set, as opposed to the sample sets with the highest water-
557 soluble aerosol concentrations, could have led to greater wet scavenging of aerosol. This case
558 also had the lowest overall mass concentration of water-soluble organic species, a low percent
559 contribution of oxalate to the water-soluble organics, and a high percent contribution of maleate.
560 This result points to the relative importance of locally-emitted species that have not yet
561 undergone photochemical and aqueous processing mechanisms that lead to the degradation of
562 longer-chain dicarboxylic acid species into oxalate.

563 These results have important implications for better understanding the aerosol budget and
564 influences in and around the Philippines and SE Asia. Transport of aerosol both into and out of
565 Metro Manila can impact human health, cloud condensation nuclei (CCN) budgets, and radiative
566 forcing in the region. Furthermore, the identification of various tracer species (e.g. K and Rb for
567 biomass burning) and the impacts of different long-range transport mechanisms have worldwide
568 applications. In addition, the mixing of different air mass types, resulting in changes in aerosol
569 characteristics (e.g. enhanced oxalate in emissions from continental regions, enhanced MSA
570 during periods of biomass burning influence), is a subject that requires more attention on a global
571 basis. While this work has shown the influence of mixing biomass burning emissions and urban
572 emissions, from both local and more distant urban centers, additional analysis at the study site
573 has demonstrated the influences seen from the mixing of sea salt aerosol with other airmasses
574 (AzadiAghdam et al., 2019). As remote-sensing measurements in this region are notoriously
575 difficult (e.g. Reid et al., 2009, 2013), in situ and model results lend vital data to address the
576 questions surrounding characteristics of aerosol that are transported into and out of this highly-
577 populated region. Measurements from in situ airborne campaigns, such as CAMP²Ex, can further
578 address the changes in aerosol physicochemical characteristics that occur during long-range
579 transport and aging in the atmosphere in the region.

580

581 *Data availability:* All data used in this work are available upon request.

582

583 *Author Contribution:* MTC, MOC, JBS, RAB, ABM, CS, and AS designed the experiments and
584 all co-authors carried out some aspect of the data collection. MTC, RAB, CS, and AS conducted
585 data analysis and interpretation. RAB and AS prepared the manuscript with contributions from
586 all co-authors.

587

588 *Competing interests:* The authors declare that they have no conflict of interest.

589

590 *Acknowledgements:* This research was funded by NASA grant 80NSSC18K0148. R. A. Braun
591 acknowledges support from the ARCS Foundation. M. T. Cruz acknowledges support from the
592 Philippine Department of Science and Technology's ASTHRD Program. A. B. MacDonald
593 acknowledges support from the Mexican National Council for Science and Technology
594 (CONACYT). We acknowledge Agilent Technologies for their support and Shane Snyder's
595 laboratories for ICP-QQQ data.

596

597 **References**

598

599 Aggarwal, S. G., and Kawamura, K.: Molecular distributions and stable carbon isotopic
600 compositions of dicarboxylic acids and related compounds in aerosols from Sapporo, Japan:

601 Implications for photochemical aging during long-range atmospheric transport, *J. Geophys. Res.-*
602 *Atmos.*, 113, 10.1029/2007jd009365, 2008.

603

604 Agrawal, H., Malloy, Q. G. J., Welch, W. A., Wayne Miller, J., and Cocker, D. R.: In-use
605 gaseous and particulate matter emissions from a modern ocean going container vessel, *Atmos.*
606 *Environ.*, 42, 5504-5510, <https://doi.org/10.1016/j.atmosenv.2008.02.053>, 2008.

607

608 Akagi, S. K., Craven, J. S., Taylor, J. W., McMeeking, G. R., Yokelson, R. J., Burling, I. R.,
609 Urbanski, S. P., Wold, C. E., Seinfeld, J. H., Coe, H., Alvarado, M. J., and Weise, D. R.:
610 Evolution of trace gases and particles emitted by a chaparral fire in California, *Atmos. Chem.*
611 *Phys.*, 12, 1397-1421, 10.5194/acp-12-1397-2012, 2012.

612

613 Alas, H. D., Müller, T., Birmili, W., Kecorius, S., Cambaliza, M. O., Simpas, J. B. B., Cayetano,
614 M., Weinhold, K., Vallar, E., Galvez, M. C., and Wiedensohler, A.: Spatial Characterization of
615 Black Carbon Mass Concentration in the Atmosphere of a Southeast Asian Megacity: An Air
616 Quality Case Study for Metro Manila, Philippines, *Aerosol Air Qual. Res.*, 18, 2301-2317,
617 10.4209/aaqr.2017.08.0281, 2018.

618

619 Allen, A. G., Nemitz, E., Shi, J. P., Harrison, R. M., and Greenwood, J. C.: Size distributions of
620 trace metals in atmospheric aerosols in the United Kingdom, *Atmos. Environ.*, 35, 4581-4591,
621 [https://doi.org/10.1016/S1352-2310\(01\)00190-X](https://doi.org/10.1016/S1352-2310(01)00190-X), 2001.

622

623 Amato, F., Pandolfi, M., Viana, M., Querol, X., Alastuey, A., and Moreno, T.: Spatial and
624 chemical patterns of PM₁₀ in road dust deposited in urban environment, *Atmos. Environ.*, 43,
625 1650-1659, <https://doi.org/10.1016/j.atmosenv.2008.12.009>, 2009.

626

627 Andreae, M. O.: Soot Carbon and Excess Fine Potassium: Long-Range Transport of
628 Combustion-Derived Aerosols, *Science*, 220, 1148, 10.1126/science.220.4602.1148, 1983.

629

630 Arimoto, R., Duce, R. A., Ray, B. J., Ellis Jr, W. G., Cullen, J. D., and Merrill, J. T.: Trace
631 elements in the atmosphere over the North Atlantic, *J. Geophys. Res.-Atmos.*, 100, 1199-1213,
632 10.1029/94jd02618, 1995.

633

634 Artaxo, P., Gerab, F., Yamasoe, M. A., and Martins, J. V.: Fine mode aerosol composition at
635 three long-term atmospheric monitoring sites in the Amazon Basin, *J. Geophys. Res.-Atmos.*, 99,
636 22857-22868, 10.1029/94jd01023, 1994.

637

638 Artaxo, P., Oyola, P., and Martinez, R.: Aerosol composition and source apportionment in
639 Santiago de Chile, *Nucl. Instrum. Meth. B*, 150, 409-416, [https://doi.org/10.1016/S0168-](https://doi.org/10.1016/S0168-583X(98)01078-7)
640 [583X\(98\)01078-7](https://doi.org/10.1016/S0168-583X(98)01078-7), 1999.

641

642 Atwood, S. A., Reid, J. S., Kreidenweis, S. M., Cliff, S. S., Zhao, Y., Lin, N.-H., Tsay, S.-C.,
643 Chu, Y.-C., and Westphal, D. L.: Size resolved measurements of springtime aerosol particles
644 over the northern South China Sea, *Atmos. Environ.*, 78, 134-143,
645 <https://doi.org/10.1016/j.atmosenv.2012.11.024>, 2013.

646

647 Atwood, S. A., Reid, J. S., Kreidenweis, S. M., Blake, D. R., Jonsson, H. H., Lagrosas, N. D.,
648 Xian, P., Reid, E. A., Sessions, W. R., and Simpas, J. B.: Size-resolved aerosol and cloud
649 condensation nuclei (CCN) properties in the remote marine South China Sea – Part 1:
650 Observations and source classification, *Atmos. Chem. Phys.*, 17, 1105-1123, 10.5194/acp-17-
651 1105-2017, 2017.

652
653 AzadiAghdam, M., Braun, R. A., Edwards, E.-L., Bañaga, P. A., Cruz, M. T., Betito, G.,
654 Cambaliza, M. O., Dadashazar, H., Lorenzo, G. R., Ma, L., MacDonald, A. B., Nguyen, P.,
655 Simpas, J. B., Stahl, C., and Sorooshian, A.: On the nature of sea salt aerosol at a coastal
656 megacity: Insights from Manila, Philippines in Southeast Asia, *Atmos. Environ.*, 216, 116922,
657 <https://doi.org/10.1016/j.atmosenv.2019.116922>, 2019.

658 Bagtasa, G.: Effect of Synoptic Scale Weather Disturbance to Philippine Transboundary Oxone
659 Pollution using WRF-CHEM. *Int. J. Environ. Sci. Dev.*, 2, 402-405,
660 10.7763/IJESD.2011.V2.159, 2011.

661
662 Bagtasa, G., Cayetano, M. G., and Yuan, C. S.: Seasonal variation and chemical characterization
663 of PM_{2.5} in northwestern Philippines, *Atmos. Chem. Phys.*, 18, 4965-4980, 10.5194/acp-18-
664 4965-2018, 2018.

665
666 Balla, D., Voutsas, D., and Samara, C.: Study of polar organic compounds in airborne particulate
667 matter of a coastal urban city, *Environ. Sci. Pollut. R.*, 25, 12191-12205, 10.1007/s11356-017-
668 9993-2, 2018.

669
670 Bautista, A. T., Pabroa, P. C. B., Santos, F. L., Racho, J. M. D., and Quirit, L. L.: Carbonaceous
671 particulate matter characterization in an urban and a rural site in the Philippines, *Atmos. Pollut.*
672 *Res.*, 5, 245-252, <https://doi.org/10.5094/APR.2014.030>, 2014.

673
674 Bovallius, A., Bucht, B., Roffey, R., and Anäs, P.: Long-range air transmission of bacteria, *Appl.*
675 *Environ. Microb.*, 35, 1231, 1978.

676
677 Braun, R. A., Dadashazar, H., MacDonald, A. B., Aldhaif, A. M., Maudlin, L. C., Crosbie, E.,
678 Aghdam, M. A., Hossein Mardi, A., and Sorooshian, A.: Impact of Wildfire Emissions on
679 Chloride and Bromide Depletion in Marine Aerosol Particles, *Environ. Sci. Technol.*, 51, 9013-
680 9021, 10.1021/acs.est.7b02039, 2017.

681
682 Brito, J., Freney, E., Dominutti, P., Borbon, A., Haslett, S. L., Batenburg, A. M., Colomb, A.,
683 Dupuy, R., Denjean, C., Burnet, F., Bourriane, T., Deroubaix, A., Sellegri, K., Borrmann, S.,
684 Coe, H., Flamant, C., Knippertz, P., and Schwarzenboeck, A.: Assessing the role of
685 anthropogenic and biogenic sources on PM₁ over southern West Africa using aircraft
686 measurements, *Atmos. Chem. Phys.*, 18, 757-772, 10.5194/acp-18-757-2018, 2018.

687
688 Campbell, J. R., Reid, J. S., Westphal, D. L., Zhang, J., Tackett, J. L., Chew, B. N., Welton, E. J.,
689 Shimizu, A., Sugimoto, N., Aoki, K., and Winker, D. M.: Characterizing the vertical profile of
690 aerosol particle extinction and linear depolarization over Southeast Asia and the Maritime

691 Continent: The 2007–2009 view from CALIOP, *Atmos. Res.*, 122, 520-543,
692 <https://doi.org/10.1016/j.atmosres.2012.05.007>, 2013.
693

694 Cao, F., Zhang, S.-C., Kawamura, K., Liu, X., Yang, C., Xu, Z., Fan, M., Zhang, W., Bao, M.,
695 Chang, Y., Song, W., Liu, S., Lee, X., Li, J., Zhang, G., and Zhang, Y.-L.: Chemical
696 characteristics of dicarboxylic acids and related organic compounds in PM_{2.5} during biomass-
697 burning and non-biomass-burning seasons at a rural site of Northeast China, *Environ. Pollut.*,
698 231, 654-662, <https://doi.org/10.1016/j.envpol.2017.08.045>, 2017.
699

700 Cayan, E. O., Chen, T.-C., Argete, J. C., Yen, M.-C., and Nilo, P. D.: The Effect of Tropical
701 Cyclones on Southwest Monsoon Rainfall in the Philippines, *J. Meteorol. Soc. Jpn. Ser. II*, 89A,
702 123-139, 10.2151/jmsj.2011-A08, 2011.
703

704 Chang, L. T.-C., Tsai, J.-H., Lin, J.-M., Huang, Y.-S., and Chiang, H.-L.: Particulate matter and
705 gaseous pollutants during a tropical storm and air pollution episode in Southern Taiwan, *Atmos.*
706 *Res.*, 99, 67-79, <https://doi.org/10.1016/j.atmosres.2010.09.002>, 2011.
707

708 Cheng, C., Li, M., Chan, C. K., Tong, H., Chen, C., Chen, D., Wu, D., Li, L., Wu, C., Cheng, P.,
709 Gao, W., Huang, Z., Li, X., Zhang, Z., Fu, Z., Bi, Y., and Zhou, Z.: Mixing state of oxalic acid
710 containing particles in the rural area of Pearl River Delta, China: implications for the formation
711 mechanism of oxalic acid, *Atmos. Chem. Phys.*, 17, 9519-9533, 10.5194/acp-17-9519-2017,
712 2017.
713

714 Chow, J. C., Watson, J. G., Kuhns, H., Etyemezian, V., Lowenthal, D. H., Crow, D., Kohl, S. D.,
715 Engelbrecht, J. P., and Green, M. C.: Source profiles for industrial, mobile, and area sources in
716 the Big Bend Regional Aerosol Visibility and Observational study, *Chemosphere*, 54, 185-208,
717 <https://doi.org/10.1016/j.chemosphere.2003.07.004>, 2004.
718

719 Chuang, M.-T., Chang, S.-C., Lin, N.-H., Wang, J.-L., Sheu, G.-R., Chang, Y.-J., and Lee, C.-T.:
720 Aerosol chemical properties and related pollutants measured in Dongsha Island in the northern
721 South China Sea during 7-SEAS/Dongsha Experiment, *Atmos. Environ.*, 78, 82-92,
722 <https://doi.org/10.1016/j.atmosenv.2012.05.014>, 2013.
723

724 Crahan, K. K., Hegg, D., Covert, D. S., and Jonsson, H.: An exploration of aqueous oxalic acid
725 production in the coastal marine atmosphere, *Atmos. Environ.*, 38, 3757-3764,
726 <https://doi.org/10.1016/j.atmosenv.2004.04.009>, 2004.
727

728 Cruz, F. T., Narisma, G. T., Villafuerte, M. Q., Cheng Chua, K. U., and Olaguera, L. M.: A
729 climatological analysis of the southwest monsoon rainfall in the Philippines, *Atmos. Res.*, 122,
730 609-616, <https://doi.org/10.1016/j.atmosres.2012.06.010>, 2013.
731

732 Cruz, M. T., Bañaga, P. A., Betito, G., Braun, R. A., Stahl, C., Aghdam, M. A., Cambaliza, M.
733 O., Dadashazar, H., Hilario, M. R., Lorenzo, G. R., Ma, L., MacDonald, A. B., Pabroa, P. C.,
734 Yee, J. R., Simpás, J. B., and Sorooshian, A.: Size-resolved Composition and Morphology of
735 Particulate Matter During the Southwest Monsoon in Metro Manila, Philippines, *Atmos. Chem.*
736 *Phys.*, 19, 10675-10696, <https://doi.org/10.5194/acp-19-10675-2019>, 2019.

737
738 Dave, P., Bhushan, M., and Venkataraman, C.: Aerosols cause intraseasonal short-term
739 suppression of Indian monsoon rainfall, *Sci. Rep.-UK*, 7, 17347, 10.1038/s41598-017-17599-1,
740 2017.
741
742 Deshmukh, D. K., Deb, M. K., Hopke, P. K., and Tsai, Y. I.: Seasonal Characteristics of Water-
743 Soluble Dicarboxylates Associated with PM10 in the Urban Atmosphere of Durg City, India,
744 *Aerosol Air Qual. Res.*, 12, 683-696, 10.4209/aaqr.2012.02.0040, 2012.
745
746 Deshmukh, D. K., Mozammel Haque, M., Kawamura, K., and Kim, Y.: Dicarboxylic acids,
747 oxocarboxylic acids and α -dicarbonyls in fine aerosols over central Alaska: Implications for
748 sources and atmospheric processes, *Atmos. Res.*, 202, 128-139,
749 <https://doi.org/10.1016/j.atmosres.2017.11.003>, 2018.
750
751 Duce, R. A., Liss, P. S., Merrill, J. T., Atlas, E. L., Buat-Menard, P., Hicks, B. B., Miller, J. M.,
752 Prospero, J. M., Arimoto, R., Church, T. M., Ellis, W., Galloway, J. N., Hansen, L., Jickells, T.
753 D., Knap, A. H., Reinhardt, K. H., Schneider, B., Soudine, A., Tokos, J. J., Tsunogai, S.,
754 Wollast, R., and Zhou, M.: The atmospheric input of trace species to the world ocean, *Global*
755 *Biogeochem. Cy.*, 5, 193-259, 10.1029/91gb01778, 1991.
756
757 Echalar, F., Gaudichet, A., Cachier, H., and Artaxo, P.: Aerosol emissions by tropical forest and
758 savanna biomass burning: Characteristic trace elements and fluxes, *Geophys. Res. Lett.*, 22,
759 3039-3042, 10.1029/95gl03170, 1995.
760
761 Ervens, B.: Modeling the Processing of Aerosol and Trace Gases in Clouds and Fogs, *Chem.*
762 *Rev.*, 115, 4157-4198, 10.1021/cr5005887, 2015.
763
764 Ervens, B., Feingold, G., Frost, G. J., and Kreidenweis, S. M.: A modeling study of aqueous
765 production of dicarboxylic acids: 1. Chemical pathways and speciated organic mass production,
766 *J. Geophys. Res.-Atmos.*, 109, 10.1029/2003jd004387, 2004.
767
768 Ervens, B., Sorooshian, A., Aldhaif, A. M., Shingler, T., Crosbie, E., Ziemba, L., Campuzano-
769 Jost, P., Jimenez, J. L., and Wisthaler, A.: Is there an aerosol signature of chemical cloud
770 processing?, *Atmos. Chem. Phys.*, 18, 16099-16119, 10.5194/acp-18-16099-2018, 2018.
771
772 Falkovich, A. H., Graber, E. R., Schkolnik, G., Rudich, Y., Maenhaut, W., and Artaxo, P.: Low
773 molecular weight organic acids in aerosol particles from Rondônia, Brazil, during the biomass-
774 burning, transition and wet periods, *Atmos. Chem. Phys.*, 5, 781-797, 10.5194/acp-5-781-2005,
775 2005.
776
777 Fang, G.-C., Lin, S.-J., Chang, S.-Y., and Chou, C.-C. K.: Effect of typhoon on atmospheric
778 particulates in autumn in central Taiwan, *Atmos. Environ.*, 43, 6039-6048,
779 <https://doi.org/10.1016/j.atmosenv.2009.08.033>, 2009.
780
781 Farren, N. J., Dunmore, R. E., Mead, M. I., Mohd Nadzir, M. S., Samah, A. A., Phang, S. M.,
782 Bandy, B. J., Sturges, W. T., and Hamilton, J. F.: Chemical characterisation of water-soluble

783 ions in atmospheric particulate matter on the east coast of Peninsular Malaysia, *Atmos. Chem.*
784 *Phys.*, 19, 1537-1553, 10.5194/acp-19-1537-2019, 2019.

785

786 Flannigan, M. D., Krawchuk, M. A., de Groot, W. J., Wotton, B. M., and Gowman, L. M.:
787 Implications of changing climate for global wildland fire, *Int. J. Wildland Fire*, 18, 483-507,
788 <https://doi.org/10.1071/WF08187>, 2009.

789

790 Flannigan, M., Cantin, A. S., de Groot, W. J., Wotton, M., Newbery, A., and Gowman, L. M.:
791 Global wildland fire season severity in the 21st century, *Forest Ecol. Manag.*, 294, 54-61,
792 <https://doi.org/10.1016/j.foreco.2012.10.022>, 2013.

793

794 Fujimori, T., Takigami, H., Agusa, T., Eguchi, A., Bekki, K., Yoshida, A., Terazono, A., and
795 Ballesteros, F. C.: Impact of metals in surface matrices from formal and informal electronic-
796 waste recycling around Metro Manila, the Philippines, and intra-Asian comparison, *J. Hazard.*
797 *Mater.*, 221-222, 139-146, <https://doi.org/10.1016/j.jhazmat.2012.04.019>, 2012.

798

799 Fung, Y. S., and Wong, L. W. Y.: Apportionment of air pollution sources by receptor models in
800 Hong Kong, *Atmos. Environ.*, 29, 2041-2048, [https://doi.org/10.1016/1352-2310\(94\)00239-H](https://doi.org/10.1016/1352-2310(94)00239-H),
801 1995.

802

803 Gadde, B., Bonnet, S., Menke, C., and Garivait, S.: Air pollutant emissions from rice straw open
804 field burning in India, Thailand and the Philippines, *Environ. Pollut.*, 157, 1554-1558,
805 <https://doi.org/10.1016/j.envpol.2009.01.004>, 2009.

806

807 Ge, C., Wang, J., Reid, J. S., Posselt, D. J., Xian, P., and Hyer, E.: Mesoscale modeling of smoke
808 transport from equatorial Southeast Asian Maritime Continent to the Philippines: First
809 comparison of ensemble analysis with in situ observations, *J. Geophys. Res.-Atmos.*, 122, 5380-
810 5398, doi:10.1002/2016JD026241, 2017.

811

812 Gelaro, R., McCarty, W., Suárez, M. J., Todling, R., Molod, A., Takacs, L., Randles, C. A.,
813 Darmenov, A., Bosilovich, M. G., Reichle, R., Wargan, K., Coy, L., Cullather, R., Draper, C.,
814 Akella, S., Buchard, V., Conaty, A., Silva, A. M. d., Gu, W., Kim, G.-K., Koster, R., Lucchesi,
815 R., Merkova, D., Nielsen, J. E., Partyka, G., Pawson, S., Putman, W., Rienecker, M., Schubert,
816 S. D., Sienkiewicz, M., and Zhao, B.: The Modern-Era Retrospective Analysis for Research and
817 Applications, Version 2 (MERRA-2), *J. Climate*, 30, 5419-5454, 10.1175/jcli-d-16-0758.1,
818 2017.

819

820 Global Modeling and Assimilation Office (GMAO): MERRA-2 inst3_3d_asm_Nv: 3d,3-
821 Hourly,Instantaneous,Model-Level,Assimilation,Assimilated Meteorological Fields V5.12.4,
822 Goddard Earth Sciences Data and Information Services Center (GES DISC),
823 10.5067/WWQSQ8IVFW8, 2015a.

824

825 Global Modeling and Assimilation Office (GMAO): MERRA-2 tavg1_2d_rad_Nx: 2d,1-
826 Hourly,Time-Averaged,Single-Level,Assimilation,Radiation Diagnostics V5.12.4, Goddard
827 Earth Sciences Data and Information Services Center (GES DISC), 10.5067/Q9QMY5PBNV1T,
828 2015b.

829
830 Goldstein, A. H., Koven, C. D., Heald, C. L., and Fung, I. Y.: Biogenic carbon and
831 anthropogenic pollutants combine to form a cooling haze over the southeastern United States, P.
832 Natl. Acad. Sci. USA, 106, 8835-8840, [10.1073/pnas.0904128106](https://doi.org/10.1073/pnas.0904128106), 2009.
833
834 Graf, H. F., Yang, J., and Wagner, T. M.: Aerosol effects on clouds and precipitation during the
835 1997 smoke episode in Indonesia, *Atmos. Chem. Phys.*, 9, 743-756, [10.5194/acp-9-743-2009](https://doi.org/10.5194/acp-9-743-2009),
836 2009.
837
838 Ho, K. F., Lee, S. C., Cao, J. J., Kawamura, K., Watanabe, T., Cheng, Y., and Chow, J. C.:
839 Dicarboxylic acids, ketocarboxylic acids and dicarbonyls in the urban roadside area of Hong
840 Kong, *Atmos. Environ.*, 40, 3030-3040, <https://doi.org/10.1016/j.atmosenv.2005.11.069>, 2006.
841
842 Hogan, T. F., Liu, M., Ridout, J. A., Peng, M. S., Whitcomb, T. R., Ruston, B. C., Reynolds, C.
843 A., Eckermann, S. D., Moskaitis, J. R., Baker, N. L., McCormack, J. P., Viner, K. C., McLay, J.
844 G., Flatau, M. K., Xu, L., Chen, C., and Chang, S. W.: The Navy Global Environmental Model,
845 *Oceanography*, 27, 116-125, <https://doi.org/10.5670/oceanog.2014.73>, 2014.
846
847 Hong, Y., Hsu, K.-L., Sorooshian, S., and Gao, X.: Precipitation Estimation from Remotely
848 Sensed Imagery Using an Artificial Neural Network Cloud Classification System, *J. Appl.*
849 *Meteorol.*, 43, 1834-1853, [10.1175/jam2173.1](https://doi.org/10.1175/jam2173.1), 2004.
850
851 Hoque, M. M. M., Kawamura, K., and Uematsu, M.: Spatio-temporal distributions of
852 dicarboxylic acids, ω -oxocarboxylic acids, pyruvic acid, α -dicarbonyls and fatty acids in the
853 marine aerosols from the North and South Pacific, *Atmos. Res.*, 185, 158-168,
854 <https://doi.org/10.1016/j.atmosres.2016.10.022>, 2017.
855
856 Hsieh, L.-Y., Kuo, S.-C., Chen, C.-L., and Tsai, Y. I.: Origin of low-molecular-weight
857 dicarboxylic acids and their concentration and size distribution variation in suburban aerosol,
858 *Atmos. Environ.*, 41, 6648-6661, <https://doi.org/10.1016/j.atmosenv.2007.04.014>, 2007.
859
860 Hsieh, L.-Y., Chen, C.-L., Wan, M.-W., Tsai, C.-H., and Tsai, Y. I.: Speciation and temporal
861 characterization of dicarboxylic acids in PM_{2.5} during a PM episode and a period of non-
862 episodic pollution, *Atmos. Environ.*, 42, 6836-6850,
863 <https://doi.org/10.1016/j.atmosenv.2008.05.021>, 2008.
864
865 Hyder, M., Genberg, J., Sandahl, M., Swietlicki, E., and Jönsson, J. Å.: Yearly trend of
866 dicarboxylic acids in organic aerosols from south of Sweden and source attribution, *Atmos.*
867 *Environ.*, 57, 197-204, <https://doi.org/10.1016/j.atmosenv.2012.04.027>, 2012.
868
869 Jeong, C.-H., Wang, J. M., Hilker, N., Debosz, J., Sofowote, U., Su, Y., Noble, M., Healy, R. M.,
870 Munoz, T., Dabek-Zlotorzynska, E., Celo, V., White, L., Audette, C., Herod, D., and Evans, G.
871 J.: Temporal and spatial variability of traffic-related PM_{2.5} sources: Comparison of exhaust and
872 non-exhaust emissions, *Atmos. Environ.*, 198, 55-69,
873 <https://doi.org/10.1016/j.atmosenv.2018.10.038>, 2019.
874

875 Juneng, L., Latif, M. T., and Tangang, F.: Factors influencing the variations of PM10 aerosol
876 dust in Klang Valley, Malaysia during the summer, *Atmos. Environ.*, 45, 4370-4378,
877 <https://doi.org/10.1016/j.atmosenv.2011.05.045>, 2011.
878

879 Kawamura, K., and Ikushima, K.: Seasonal changes in the distribution of dicarboxylic acids in
880 the urban atmosphere, *Environ. Sci. Technol.*, 27, 2227-2235, 10.1021/es00047a033, 1993.
881

882 Kawamura, K., and Kaplan, I. R.: Motor exhaust emissions as a primary source for dicarboxylic
883 acids in Los Angeles ambient air, *Environ. Sci. Technol.*, 21, 105-110, 10.1021/es00155a014,
884 1987.
885

886 Kawamura, K., and Sakaguchi, F.: Molecular distributions of water soluble dicarboxylic acids in
887 marine aerosols over the Pacific Ocean including tropics, *J. Geophys. Res.-Atmos.*, 104, 3501-
888 3509, 10.1029/1998jd100041, 1999.
889

890 Kawamura, K., Kasukabe, H., and Barrie, L. A.: Source and reaction pathways of dicarboxylic
891 acids, ketoacids and dicarbonyls in arctic aerosols: One year of observations, *Atmos. Environ.*,
892 30, 1709-1722, [https://doi.org/10.1016/1352-2310\(95\)00395-9](https://doi.org/10.1016/1352-2310(95)00395-9), 1996.
893

894 Kecorius, S., Madueño, L., Vallar, E., Alas, H., Betito, G., Birmili, W., Cambaliza, M. O.,
895 Catipay, G., Gonzaga-Cayetano, M., Galvez, M. C., Lorenzo, G., Müller, T., Simpas, J. B.,
896 Tamayo, E. G., and Wiedensohler, A.: Aerosol particle mixing state, refractory particle number
897 size distributions and emission factors in a polluted urban environment: Case study of Metro
898 Manila, Philippines, *Atmos. Environ.*, 170, 169-183,
899 <https://doi.org/10.1016/j.atmosenv.2017.09.037>, 2017.
900

901 Kim, E., and Hopke, P. K.: Source characterization of ambient fine particles at multiple sites in
902 the Seattle area, *Atmos. Environ.*, 42, 6047-6056,
903 <https://doi.org/10.1016/j.atmosenv.2008.03.032>, 2008.
904

905 Kim, J. Y., Ghim, Y. S., Song, C. H., Yoon, S.-C., and Han, J. S.: Seasonal characteristics of air
906 masses arriving at Gosan, Korea, using fine particle measurements between November 2001 and
907 August 2003, *J. Geophys. Res.-Atmos.*, 112, 10.1029/2005jd006946, 2007.
908

909 Kim Oanh, N. T., Upadhyay, N., Zhuang, Y. H., Hao, Z. P., Murthy, D. V. S., Lestari, P.,
910 Villarin, J. T., Chengchua, K., Co, H. X., Dung, N. T., and Lindgren, E. S.: Particulate air
911 pollution in six Asian cities: Spatial and temporal distributions, and associated sources, *Atmos.*
912 *Environ.*, 40, 3367-3380, <https://doi.org/10.1016/j.atmosenv.2006.01.050>, 2006.
913

914 Kristiansen, N. I., Stohl, A., Olivie, D. J. L., Croft, B., Søvde, O. A., Klein, H., Christoudias, T.,
915 Kunkel, D., Leadbetter, S. J., Lee, Y. H., Zhang, K., Tsigaridis, K., Bergman, T., Evangelidou, N.,
916 Wang, H., Ma, P. L., Easter, R. C., Rasch, P. J., Liu, X., Pitari, G., Di Genova, G., Zhao, S. Y.,
917 Balkanski, Y., Bauer, S. E., Faluvegi, G. S., Kokkola, H., Martin, R. V., Pierce, J. R., Schulz, M.,
918 Shindell, D., Tost, H., and Zhang, H.: Evaluation of observed and modelled aerosol lifetimes
919 using radioactive tracers of opportunity and an ensemble of 19 global models, *Atmos. Chem.*
920 *Phys.*, 16, 3525-3561, 10.5194/acp-16-3525-2016, 2016.

921
922 Kumar, S., Aggarwal, S. G., Gupta, P. K., and Kawamura, K.: Investigation of the tracers for
923 plastic-enriched waste burning aerosols, *Atmos. Environ.*, 108, 49-58,
924 <https://doi.org/10.1016/j.atmosenv.2015.02.066>, 2015.
925
926 Kunwar, B., Kawamura, K., Fujiwara, S., Fu, P., Miyazaki, Y., and Pokhrel, A.: Dicarboxylic
927 acids, oxocarboxylic acids and α -dicarbonyls in atmospheric aerosols from Mt. Fuji, Japan:
928 Implication for primary emission versus secondary formation, *Atmos. Res.*, 221, 58-71,
929 <https://doi.org/10.1016/j.atmosres.2019.01.021>, 2019.
930
931 Latif, M. T., Othman, M., Idris, N., Juneng, L., Abdullah, A. M., Hamzah, W. P., Khan, M. F.,
932 Nik Sulaiman, N. M., Jewaratnam, J., Aghamohammadi, N., Sahani, M., Xiang, C. J., Ahamad,
933 F., Amil, N., Darus, M., Varkkey, H., Tangang, F., and Jaafar, A. B.: Impact of regional haze
934 towards air quality in Malaysia: A review, *Atmos. Environ.*, 177, 28-44,
935 <https://doi.org/10.1016/j.atmosenv.2018.01.002>, 2018.
936
937 Li, X.-d., Yang, Z., Fu, P., Yu, J., Lang, Y.-c., Liu, D., Ono, K., and Kawamura, K.: High
938 abundances of dicarboxylic acids, oxocarboxylic acids, and α -dicarbonyls in fine aerosols
939 (PM_{2.5}) in Chengdu, China during wintertime haze pollution, *Environ. Sci. Pollut. R.*, 22,
940 12902-12918, [10.1007/s11356-015-4548-x](https://doi.org/10.1007/s11356-015-4548-x), 2015.
941
942 Lin, C.-C., Chen, S.-J., Huang, K.-L., Hwang, W.-I., Chang-Chien, G.-P., and Lin, W.-Y.:
943 Characteristics of Metals in Nano/Ultrafine/Fine/Coarse Particles Collected Beside a Heavily
944 Trafficked Road, *Environ. Sci. Technol.*, 39, 8113-8122, [10.1021/es048182a](https://doi.org/10.1021/es048182a), 2005.
945
946 Lin, C. Y., Hsu, H. m., Lee, Y. H., Kuo, C. H., Sheng, Y. F., and Chu, D. A.: A new transport
947 mechanism of biomass burning from Indochina as identified by modeling studies, *Atmos. Chem.*
948 *Phys.*, 9, 7901-7911, [10.5194/acp-9-7901-2009](https://doi.org/10.5194/acp-9-7901-2009), 2009.
949
950 Lin, I. I., Chen, J.-P., Wong, G. T. F., Huang, C.-W., and Lien, C.-C.: Aerosol input to the South
951 China Sea: Results from the MODerate Resolution Imaging Spectro-radiometer, the Quick
952 Scatterometer, and the Measurements of Pollution in the Troposphere Sensor, *Deep-Sea Res. Pt.*
953 *II*, 54, 1589-1601, <https://doi.org/10.1016/j.dsr2.2007.05.013>, 2007.
954
955 Lindqvist, O., Johansson, K., Bringmark, L., Timm, B., Aastrup, M., Andersson, A., Hovsenius,
956 G., Håkanson, L., Iverfeldt, Å., and Meili, M.: Mercury in the Swedish environment — Recent
957 research on causes, consequences and corrective methods, *Water Air Soil Poll.*, 55, xi-261,
958 [10.1007/bf00542429](https://doi.org/10.1007/bf00542429), 1991.
959
960 Liu, W., Han, Y., Yin, Y., Duan, J., Gong, J., Liu, Z., and Xu, W.: An aerosol air pollution
961 episode affected by binary typhoons in east and central China, *Atmos. Pollut. Res.*, 9, 634-642,
962 <https://doi.org/10.1016/j.apr.2018.01.005>, 2018.
963
964 Liu, Y., Cai, W., Sun, C., Song, H., Cobb, K. M., Li, J., Leavitt, S. W., Wu, L., Cai, Q., Liu, R.,
965 Ng, B., Cherubini, P., Büentgen, U., Song, Y., Wang, G., Lei, Y., Yan, L., Li, Q., Ma, Y., Fang,
966 C., Sun, J., Li, X., Chen, D., and Linderholm, H. W.: Anthropogenic aerosols cause recent

967 pronounced weakening of Asian Summer Monsoon relative to last four centuries, *Geophys. Res.*
968 *Letts.*, 46, 10.1029/2019gl082497, 2019.

969

970 Lu, C.-C., Yuan, C.-S., and Li, T.-C.: How Aeolian Dust Deteriorate Ambient Particulate Air
971 Quality along an Expansive River Valley in Southern Taiwan? A Case Study of Typhoon
972 Doksuri, *Aerosol Air Qual. Res.*, 17, 2181-2196, 10.4209/aaqr.2017.08.0257, 2017.

973

974 Lynch, P., Reid, J. S., Westphal, D. L., Zhang, J., Hogan, T. F., Hyer, E. J., Curtis, C. A., Hegg,
975 D. A., Shi, Y., Campbell, J. R., Rubin, J. I., Sessions, W. R., Turk, F. J., and Walker, A. L.: An
976 11-year global gridded aerosol optical thickness reanalysis (v1.0) for atmospheric and climate
977 sciences, *Geosci. Model Dev.*, 9, 1489-1522, 10.5194/gmd-9-1489-2016, 2016.

978

979 Lyons, W. A., Dooley, J. C., and Whitby, K. T.: Satellite detection of long-range pollution
980 transport and sulfate aerosol hazes, *Atmos. Environ. (1967)*, 12, 621-631,
981 [https://doi.org/10.1016/0004-6981\(78\)90242-1](https://doi.org/10.1016/0004-6981(78)90242-1), 1978.

982

983 Ma, L., Dadashazar, H., Braun, R. A., MacDonald, A. B., Aghdam, M. A., Maudlin, L. C., and
984 Sorooshian, A.: Size-resolved Characteristics of Water-Soluble Particulate Elements in a Coastal
985 Area: Source Identification, Influence of Wildfires, and Diurnal Variability, *Atmos. Environ.*,
986 <https://doi.org/10.1016/j.atmosenv.2019.02.045>, 2019.

987

988 Maenhaut, W., Salma, I., Cafmeyer, J., Annegarn, H. J., and Andreae, M. O.: Regional
989 atmospheric aerosol composition and sources in the eastern Transvaal, South Africa, and impact
990 of biomass burning, *J. Geophys. Res.-Atmos.*, 101, 23631-23650, 10.1029/95jd02930, 1996.

991

992 Maki, T., Lee, K. C., Kawai, K., Onishi, K., Hong, C. S., Kurosaki, Y., Shinoda, M., Kai, K.,
993 Iwasaka, Y., Archer, S. D. J., Lacap-Bugler, D. C., Hasegawa, H., and Pointing, S. B.: Aeolian
994 dispersal of bacteria associated with desert dust and anthropogenic particles over continental and
995 oceanic surfaces, *J. Geophys. Res.-Atmos.*, 124, 10.1029/2018jd029597, 2019.

996

997 Mamoudou, I., Zhang, F., Chen, Q., Wang, P., and Chen, Y.: Characteristics of PM_{2.5} from ship
998 emissions and their impacts on the ambient air: A case study in Yangshan Harbor, Shanghai, *Sci.*
999 *Total Environ.*, 640-641, 207-216, <https://doi.org/10.1016/j.scitotenv.2018.05.261>, 2018.

1000

1001 Marple, V., Olson, B., Romay, F., Hudak, G., Geerts, S. M., and Lundgren, D.: Second
1002 Generation Micro-Orifice Uniform Deposit Impactor, 120 MOUDI-II: Design, Evaluation, and
1003 Application to Long-Term Ambient Sampling, *Aerosol Sci. Tech.*, 48, 427-433,
1004 10.1080/02786826.2014.884274, 2014.

1005

1006 Maudlin, L. C., Wang, Z., Jonsson, H. H., and Sorooshian, A.: Impact of wildfires on size-
1007 resolved aerosol composition at a coastal California site, *Atmos. Environ.*, 119, 59-68,
1008 <https://doi.org/10.1016/j.atmosenv.2015.08.039>, 2015.

1009

1010 Mosher, B. W., and Duce, R. A.: A global atmospheric selenium budget, *J. Geophys. Res.-*
1011 *Atmos.*, 92, 13289-13298, doi:10.1029/JD092iD11p13289, 1987.

1012

1013 Nguyen, P., Sellars, S., Thorstensen, A., Tao, Y., Ashouri, H., Braithwaite, D., Hsu, K., and
1014 Sorooshian, S.: Satellites Track Precipitation of Super Typhoon Haiyan, *Eos Trans. AGU*, 95,
1015 133-135, 10.1002/2014eo160002, 2014.

1016

1017 Nguyen, P., Shearer, E. J., Tran, H., Ombadi, M., Hayatbini, N., Palacios, T., Huynh, P.,
1018 Braithwaite, D., Updegraff, G., Hsu, K., Kuligowski, B., Logan, W. S., and Sorooshian, S.: The
1019 CHRS Data Portal, an easily accessible public repository for PERSIANN global satellite
1020 precipitation data, *Scientific Data*, 6, 180296, 10.1038/sdata.2018.296, 2019.

1021

1022 Nirmalkar, J., Deshmukh, D. K., Deb, M. K., Tsai, Y. I., and Sopajaree, K.: Mass loading and
1023 episodic variation of molecular markers in PM_{2.5} aerosols over a rural area in eastern central
1024 India, *Atmos. Environ.*, 117, 41-50, <https://doi.org/10.1016/j.atmosenv.2015.07.003>, 2015.

1025

1026 Nordø, J.: Long range transport of air pollutants in Europe and acid precipitation in Norway,
1027 *Water Air Soil Poll.*, 6, 199-217, 10.1007/bf00182865, 1976.

1028

1029 Pakkanen, T. A., Loukkola, K., Korhonen, C. H., Aurela, M., Mäkelä, T., Hillamo, R. E., Aarnio,
1030 P., Koskentalo, T., Kousa, A., and Maenhaut, W.: Sources and chemical composition of
1031 atmospheric fine and coarse particles in the Helsinki area, *Atmos. Environ.*, 35, 5381-5391,
1032 [https://doi.org/10.1016/S1352-2310\(01\)00307-7](https://doi.org/10.1016/S1352-2310(01)00307-7), 2001.

1033

1034 Pakkanen, T. A., Kerminen, V.-M., Loukkola, K., Hillamo, R. E., Aarnio, P., Koskentalo, T., and
1035 Maenhaut, W.: Size distributions of mass and chemical components in street-level and rooftop
1036 PM₁ particles in Helsinki, *Atmos. Environ.*, 37, 1673-1690, [https://doi.org/10.1016/S1352-2310\(03\)00011-6](https://doi.org/10.1016/S1352-2310(03)00011-6), 2003.

1037

1038

1039 Pandolfi, M., Gonzalez-Castanedo, Y., Alastuey, A., de la Rosa, J. D., Mantilla, E., de la Campa,
1040 A. S., Querol, X., Pey, J., Amato, F., and Moreno, T.: Source apportionment of PM₁₀ and PM_{2.5}
1041 at multiple sites in the strait of Gibraltar by PMF: impact of shipping emissions, *Environ. Sci.*
1042 *Pollut. R.*, 18, 260-269, 10.1007/s11356-010-0373-4, 2011.

1043

1044 Querol, X., Alastuey, A., Moreno, T., Viana, M. M., Castillo, S., Pey, J., Rodríguez, S.,
1045 Artiñano, B., Salvador, P., Sánchez, M., Garcia Dos Santos, S., Hecce Garraleta, M. D.,
1046 Fernandez-Patier, R., Moreno-Grau, S., Negral, L., Minguillón, M. C., Monfort, E., Sanz, M. J.,
1047 Palomo-Marín, R., Pinilla-Gil, E., Cuevas, E., de la Rosa, J., and Sánchez de la Campa, A.:
1048 Spatial and temporal variations in airborne particulate matter (PM₁₀ and PM_{2.5}) across Spain
1049 1999–2005, *Atmos. Environ.*, 42, 3964-3979, <https://doi.org/10.1016/j.atmosenv.2006.10.071>,
1050 2008.

1051

1052 Ray, J., and McDow, S. R.: Dicarboxylic acid concentration trends and sampling artifacts,
1053 *Atmos. Environ.*, 39, 7906-7919, <https://doi.org/10.1016/j.atmosenv.2005.09.024>, 2005.

1054

1055 Reid, J. S., Hyer, E. J., Prins, E. M., Westphal, D. L., Zhang, J., Wang, J., Christopher, S. A.,
1056 Curtis, C. A., Schmidt, C. C., Eleuterio, D. P., Richardson, K. A., and Hoffman, J. P.: Global
1057 Monitoring and Forecasting of Biomass-Burning Smoke: Description of and Lessons From the

1058 Fire Locating and Modeling of Burning Emissions (FLAMBE) Program, *IEEE J. Sel. Top.*
1059 *Appl.*, 2, 144-162, 10.1109/jstars.2009.2027443, 2009.

1060
1061 Reid, J. S., Xian, P., Hyer, E. J., Flatau, M. K., Ramirez, E. M., Turk, F. J., Sampson, C. R.,
1062 Zhang, C., Fukada, E. M., and Maloney, E. D.: Multi-scale meteorological conceptual analysis of
1063 observed active fire hotspot activity and smoke optical depth in the Maritime Continent, *Atmos.*
1064 *Chem. Phys.*, 12, 2117-2147, 10.5194/acp-12-2117-2012, 2012.

1065
1066 Reid, J. S., Hyer, E. J., Johnson, R. S., Holben, B. N., Yokelson, R. J., Zhang, J., Campbell, J. R.,
1067 Christopher, S. A., Di Girolamo, L., Giglio, L., Holz, R. E., Kearney, C., Miettinen, J., Reid, E.
1068 A., Turk, F. J., Wang, J., Xian, P., Zhao, G., Balasubramanian, R., Chew, B. N., Janjai, S.,
1069 Lagrosas, N., Lestari, P., Lin, N.-H., Mahmud, M., Nguyen, A. X., Norris, B., Oanh, N. T. K.,
1070 Oo, M., Salinas, S. V., Welton, E. J., and Liew, S. C.: Observing and understanding the
1071 Southeast Asian aerosol system by remote sensing: An initial review and analysis for the Seven
1072 Southeast Asian Studies (7SEAS) program, *Atmos. Res.*, 122, 403-468,
1073 <https://doi.org/10.1016/j.atmosres.2012.06.005>, 2013.

1074
1075 Reid, J. S., Lagrosas, N. D., Jonsson, H. H., Reid, E. A., Sessions, W. R., Simpas, J. B., Uy, S.
1076 N., Boyd, T. J., Atwood, S. A., Blake, D. R., Campbell, J. R., Cliff, S. S., Holben, B. N., Holz,
1077 R. E., Hyer, E. J., Lynch, P., Meinardi, S., Posselt, D. J., Richardson, K. A., Salinas, S. V.,
1078 Smirnov, A., Wang, Q., Yu, L., and Zhang, J.: Observations of the temporal variability in aerosol
1079 properties and their relationships to meteorology in the summer monsoonal South China Sea/East
1080 Sea: the scale-dependent role of monsoonal flows, the Madden–Julian Oscillation, tropical
1081 cyclones, squall lines and cold pools, *Atmos. Chem. Phys.*, 15, 1745-1768, 10.5194/acp-15-
1082 1745-2015, 2015.

1083
1084 Reid, J. S., Xian, P., Holben, B. N., Hyer, E. J., Reid, E. A., Salinas, S. V., Zhang, J., Campbell,
1085 J. R., Chew, B. N., Holz, R. E., Kuciauskas, A. P., Lagrosas, N., Posselt, D. J., Sampson, C. R.,
1086 Walker, A. L., Welton, E. J., and Zhang, C.: Aerosol meteorology of the Maritime Continent for
1087 the 2012 7SEAS southwest monsoon intensive study – Part 1: regional-scale phenomena, *Atmos.*
1088 *Chem. Phys.*, 16, 14041-14056, 10.5194/acp-16-14041-2016, 2016a.

1089
1090 Reid, J. S., Lagrosas, N. D., Jonsson, H. H., Reid, E. A., Atwood, S. A., Boyd, T. J., Ghate, V.
1091 P., Xian, P., Posselt, D. J., Simpas, J. B., Uy, S. N., Zaiger, K., Blake, D. R., Bucholtz, A.,
1092 Campbell, J. R., Chew, B. N., Cliff, S. S., Holben, B. N., Holz, R. E., Hyer, E. J., Kreidenweis,
1093 S. M., Kuciauskas, A. P., Lolli, S., Oo, M., Perry, K. D., Salinas, S. V., Sessions, W. R.,
1094 Smirnov, A., Walker, A. L., Wang, Q., Yu, L., Zhang, J., and Zhao, Y.: Aerosol meteorology of
1095 Maritime Continent for the 2012 7SEAS southwest monsoon intensive study – Part 2: Philippine
1096 receptor observations of fine-scale aerosol behavior, *Atmos. Chem. Phys.*, 16, 14057-14078,
1097 10.5194/acp-16-14057-2016, 2016b.

1098
1099 Ross, A. D., Holz, R. E., Quinn, G., Reid, J. S., Xian, P., Turk, F. J., and Posselt, D. J.: Exploring
1100 the first aerosol indirect effect over Southeast Asia using a 10-year collocated MODIS, CALIOP,
1101 and model dataset, *Atmos. Chem. Phys.*, 18, 12747-12764, 10.5194/acp-18-12747-2018, 2018.

1102

1103 Satsumabayashi, H., Kurita, H., Yokouchi, Y., and Ueda, H.: Photochemical formation of
 1104 particulate dicarboxylic acids under long-range transport in central Japan, *Atmos. Environ.*. Part
 1105 A. General Topics, 24, 1443-1450, [https://doi.org/10.1016/0960-1686\(90\)90053-P](https://doi.org/10.1016/0960-1686(90)90053-P), 1990.
 1106

1107 Schlosser, J. S., Braun, R. A., Bradley, T., Dadashazar, H., MacDonald, A. B., Aldhaif, A. A.,
 1108 Aghdam, M. A., Mardi, A. H., Xian, P., and Sorooshian, A.: Analysis of aerosol composition
 1109 data for western United States wildfires between 2005 and 2015: Dust emissions, chloride
 1110 depletion, and most enhanced aerosol constituents, *J. Geophys. Res.-Atmos.*, 122, 8951-8966,
 1111 10.1002/2017jd026547, 2017.
 1112

1113 Simpas, J., Lorenzo, G., and Cruz, M. T.: Monitoring Particulate Matter Levels and Composition
 1114 for Source Apportionment Study in Metro Manila, Philippines, in: *Improving Air Quality in
 1115 Asian Developing Countries: Compilation of Research Findings*, edited by: Kim Oanh, N. T.,
 1116 NARENCA, Vietnam Publishing House of Natural Resources, Environment and Cartography,
 1117 Vietnam, 239-261, 2014.
 1118

1119 Singh, M., Jaques, P. A., and Sioutas, C.: Size distribution and diurnal characteristics of particle-
 1120 bound metals in source and receptor sites of the Los Angeles Basin, *Atmos. Environ.*, 36, 1675-
 1121 1689, [https://doi.org/10.1016/S1352-2310\(02\)00166-8](https://doi.org/10.1016/S1352-2310(02)00166-8), 2002.
 1122

1123 Song, J., Zhao, Y., Zhang, Y., Fu, P., Zheng, L., Yuan, Q., Wang, S., Huang, X., Xu, W., Cao,
 1124 Z., Gromov, S., and Lai, S.: Influence of biomass burning on atmospheric aerosols over the
 1125 western South China Sea: Insights from ions, carbonaceous fractions and stable carbon isotope
 1126 ratios, *Environ. Pollut.*, 242, 1800-1809, <https://doi.org/10.1016/j.envpol.2018.07.088>, 2018.
 1127

1128 Song, X.-H., Polissar, A. V., and Hopke, P. K.: Sources of fine particle composition in the
 1129 northeastern US, *Atmos. Environ.*, 35, 5277-5286, [https://doi.org/10.1016/S1352-
 1130 2310\(01\)00338-7](https://doi.org/10.1016/S1352-2310(01)00338-7), 2001.
 1131

1132 Sorooshian, A., Varutbangkul, V., Brechtel, F. J., Ervens, B., Feingold, G., Bahreini, R.,
 1133 Murphy, S. M., Holloway, J. S., Atlas, E. L., Buzorius, G., Jonsson, H., Flagan, R. C., and
 1134 Seinfeld, J. H.: Oxalic acid in clear and cloudy atmospheres: Analysis of data from International
 1135 Consortium for Atmospheric Research on Transport and Transformation 2004, *J. Geophys. Res.-
 1136 Atmos.*, 111, 10.1029/2005jd006880, 2006.
 1137

1138 Sorooshian, A., Ng, N. L., Chan, A. W. H., Feingold, G., Flagan, R. C., and Seinfeld, J. H.:
 1139 Particulate organic acids and overall water-soluble aerosol composition measurements from the
 1140 2006 Gulf of Mexico Atmospheric Composition and Climate Study (GoMACCS), *J. Geophys.
 1141 Res.-Atmos.*, 112, 10.1029/2007jd008537, 2007a.
 1142

1143 Sorooshian, A., Lu, M.-L., Brechtel, F. J., Jonsson, H., Feingold, G., Flagan, R. C., and Seinfeld,
 1144 J. H.: On the Source of Organic Acid Aerosol Layers above Clouds, *Environ. Sci. Technol.*, 41,
 1145 4647-4654, 10.1021/es0630442, 2007b.
 1146

1147 Sorooshian, A., Crosbie, E., Maudlin, L. C., Youn, J.-S., Wang, Z., Shingler, T., Ortega, A. M.,
 1148 Hersey, S., and Woods, R. K.: Surface and airborne measurements of organosulfur and

1149 methanesulfonate over the western United States and coastal areas, *J. Geophys. Res.-Atmos.*,
1150 120, 8535-8548, 10.1002/2015jd023822, 2015.

1151

1152 Stein, A. F., Draxler, R. R., Rolph, G. D., Stunder, B. J. B., Cohen, M. D., and Ngan, F.:
1153 NOAA's HYSPLIT Atmospheric Transport and Dispersion Modeling System, *B. Am. Meteorol.*
1154 *Soc.*, 96, 2059-2077, 10.1175/bams-d-14-00110.1, 2015.

1155

1156 Sternbeck, J., Sjödin, Å., and Andréasson, K.: Metal emissions from road traffic and the
1157 influence of resuspension—results from two tunnel studies, *Atmos. Environ.*, 36, 4735-4744,
1158 [https://doi.org/10.1016/S1352-2310\(02\)00561-7](https://doi.org/10.1016/S1352-2310(02)00561-7), 2002.

1159

1160 Thepnuan, D., Chantara, S., Lee, C.-T., Lin, N.-H., and Tsai, Y. I.: Molecular markers for
1161 biomass burning associated with the characterization of PM_{2.5} and component sources during
1162 dry season haze episodes in Upper South East Asia, *Sci. Total Environ.*, 658, 708-722,
1163 <https://doi.org/10.1016/j.scitotenv.2018.12.201>, 2019.

1164

1165 Thurston, G. D., and Spengler, J. D.: A quantitative assessment of source contributions to
1166 inhalable particulate matter pollution in metropolitan Boston, *Atmos. Environ.*, 19, 9-25,
1167 [https://doi.org/10.1016/0004-6981\(85\)90132-5](https://doi.org/10.1016/0004-6981(85)90132-5), 1985.

1168

1169 Vaughan, M. A., Young, S. A., Winker, D. M., Powell, K. A., Omar, A. H., Liu, Z., Hu, Y., and
1170 Hostetler, C. A.: Fully automated analysis of space-based lidar data: an overview of the
1171 CALIPSO retrieval algorithms and data products, *Proc. SPIE*, 5575,
1172 <https://doi.org/10.1117/12.572024>, 2004.

1173

1174 Wang, H., and Shooter, D.: Low molecular weight dicarboxylic acids in PM₁₀ in a city with
1175 intensive solid fuel burning, *Chemosphere*, 56, 725-733,
1176 <https://doi.org/10.1016/j.chemosphere.2004.04.030>, 2004.

1177

1178 Wang, J., Ge, C., Yang, Z., Hyer, E. J., Reid, J. S., Chew, B.-N., Mahmud, M., Zhang, Y., and
1179 Zhang, M.: Mesoscale modeling of smoke transport over the Southeast Asian Maritime
1180 Continent: Interplay of sea breeze, trade wind, typhoon, and topography, *Atmos. Res.*, 122, 486-
1181 503, <https://doi.org/10.1016/j.atmosres.2012.05.009>, 2013.

1182

1183 Wang, S.-H., Tsay, S.-C., Lin, N.-H., Hsu, N. C., Bell, S. W., Li, C., Ji, Q., Jeong, M.-J.,
1184 Hansell, R. A., Welton, E. J., Holben, B. N., Sheu, G.-R., Chu, Y.-C., Chang, S.-C., Liu, J.-J.,
1185 and Chiang, W.-L.: First detailed observations of long-range transported dust over the northern
1186 South China Sea, *Atmos. Environ.*, 45, 4804-4808,
1187 <https://doi.org/10.1016/j.atmosenv.2011.04.077>, 2011.

1188

1189 Weber, R. J., Sullivan, A. P., Peltier, R. E., Russell, A., Yan, B., Zheng, M., de Gouw, J.,
1190 Warneke, C., Brock, C., Holloway, J. S., Atlas, E. L., and Edgerton, E.: A study of secondary
1191 organic aerosol formation in the anthropogenic-influenced southeastern United States, *J.*
1192 *Geophys. Res.-Atmos.*, 112, 10.1029/2007jd008408, 2007.

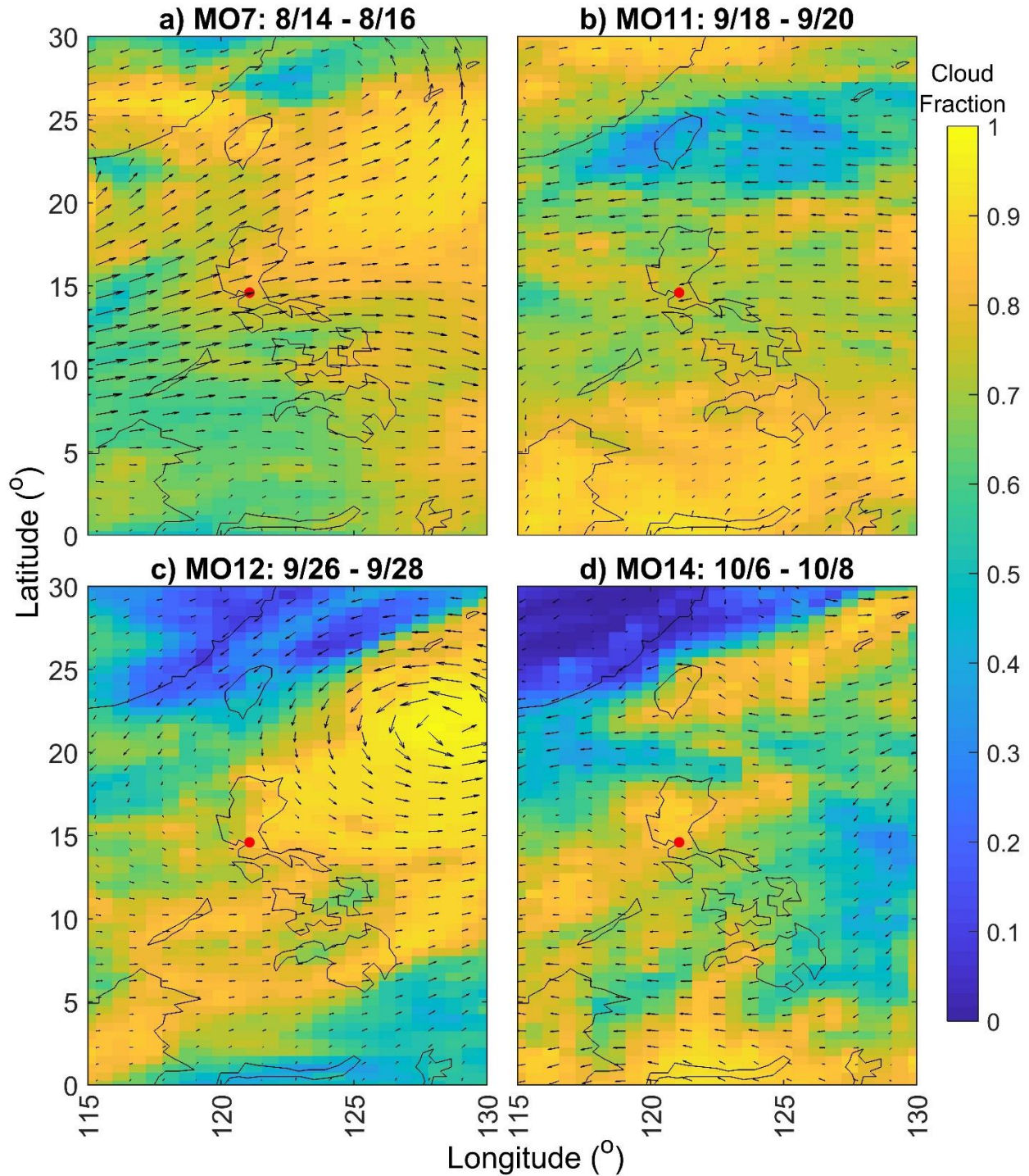
1193

1194 Wen, H., and Carignan, J.: Reviews on atmospheric selenium: Emissions, speciation and fate,
1195 Atmos. Environ., 41, 7151-7165, <https://doi.org/10.1016/j.atmosenv.2007.07.035>, 2007.
1196
1197 Winker, D. M., Vaughan, M. A., Omar, A., Hu, Y., Powell, K. A., Liu, Z., Hunt, W. H., and
1198 Young, S. A.: Overview of the CALIPSO Mission and CALIOP Data Processing Algorithms, J.
1199 Atmos. Ocean. Tech., 26, 2310-2323, [10.1175/2009jtech1281.1](https://doi.org/10.1175/2009jtech1281.1), 2009.
1200
1201 Wonaschuetz, A., Sorooshian, A., Ervens, B., Chuang, P. Y., Feingold, G., Murphy, S. M., de
1202 Gouw, J., Warneke, C., and Jonsson, H. H.: Aerosol and gas re-distribution by shallow cumulus
1203 clouds: An investigation using airborne measurements, J. Geophys. Res.-Atmos., 117,
1204 [10.1029/2012jd018089](https://doi.org/10.1029/2012jd018089), 2012.
1205
1206 Xian, P., Reid, J. S., Atwood, S. A., Johnson, R. S., Hyer, E. J., Westphal, D. L., and Sessions,
1207 W.: Smoke aerosol transport patterns over the Maritime Continent, Atmos. Res., 122, 469-485,
1208 <https://doi.org/10.1016/j.atmosres.2012.05.006>, 2013.
1209
1210 Xu, J., Zhang, J., Liu, J., Yi, K., Xiang, S., Hu, X., Wang, Y., Tao, S., and Ban-Weiss, G.:
1211 Influence of cloud microphysical processes on black carbon wet removal, global distributions,
1212 and radiative forcing, Atmos. Chem. Phys., 19, 1587-1603, [10.5194/acp-19-1587-2019](https://doi.org/10.5194/acp-19-1587-2019), 2019.
1213
1214 Yamasoe, M. A., Artaxo, P., Miguel, A. H., and Allen, A. G.: Chemical composition of aerosol
1215 particles from direct emissions of vegetation fires in the Amazon Basin: water-soluble species
1216 and trace elements, Atmos. Environ., 34, 1641-1653, [https://doi.org/10.1016/S1352-](https://doi.org/10.1016/S1352-2310(99)00329-5)
1217 [2310\(99\)00329-5](https://doi.org/10.1016/S1352-2310(99)00329-5), 2000.
1218
1219 Yan, J., Chen, L., Lin, Q., Zhao, S., and Zhang, M.: Effect of typhoon on atmospheric aerosol
1220 particle pollutants accumulation over Xiamen, China, Chemosphere, 159, 244-255,
1221 <https://doi.org/10.1016/j.chemosphere.2016.06.006>, 2016.
1222
1223 Yao, X., Fang, M., Chan, C. K., Ho, K. F., and Lee, S. C.: Characterization of dicarboxylic acids
1224 in PM_{2.5} in Hong Kong, Atmos. Environ., 38, 963-970,
1225 <https://doi.org/10.1016/j.atmosenv.2003.10.048>, 2004.
1226
1227 Yokelson, R. J., Crouse, J. D., DeCarlo, P. F., Karl, T., Urbanski, S., Atlas, E., Campos, T.,
1228 Shinozuka, Y., Kapustin, V., Clarke, A. D., Weinheimer, A., Knapp, D. J., Montzka, D. D.,
1229 Holloway, J., Weibring, P., Flocke, F., Zheng, W., Toohey, D., Wennberg, P. O., Wiedinmyer,
1230 C., Mauldin, L., Fried, A., Richter, D., Walega, J., Jimenez, J. L., Adachi, K., Buseck, P. R.,
1231 Hall, S. R., and Shetter, R.: Emissions from biomass burning in the Yucatan, Atmos. Chem.
1232 Phys., 9, 5785-5812, [10.5194/acp-9-5785-2009](https://doi.org/10.5194/acp-9-5785-2009), 2009.
1233
1234 Zhang, Y.-N., Zhang, Z.-S., Chan, C.-Y., Engling, G., Sang, X.-F., Shi, S., and Wang, X.-M.:
1235 Levoglucosan and carbonaceous species in the background aerosol of coastal southeast China:
1236 case study on transport of biomass burning smoke from the Philippines, Environ. Sci. Pollut. R.,
1237 19, 244-255, [10.1007/s11356-011-0548-7](https://doi.org/10.1007/s11356-011-0548-7), 2012.
1238

1239 Zhao, X., Wang, X., Ding, X., He, Q., Zhang, Z., Liu, T., Fu, X., Gao, B., Wang, Y., Zhang, Y.,
1240 Deng, X., and Wu, D.: Compositions and sources of organic acids in fine particles (PM_{2.5}) over
1241 the Pearl River Delta region, south China, *J. Environ. Sci.*, 26, 110-121,
1242 [https://doi.org/10.1016/S1001-0742\(13\)60386-1](https://doi.org/10.1016/S1001-0742(13)60386-1), 2014.

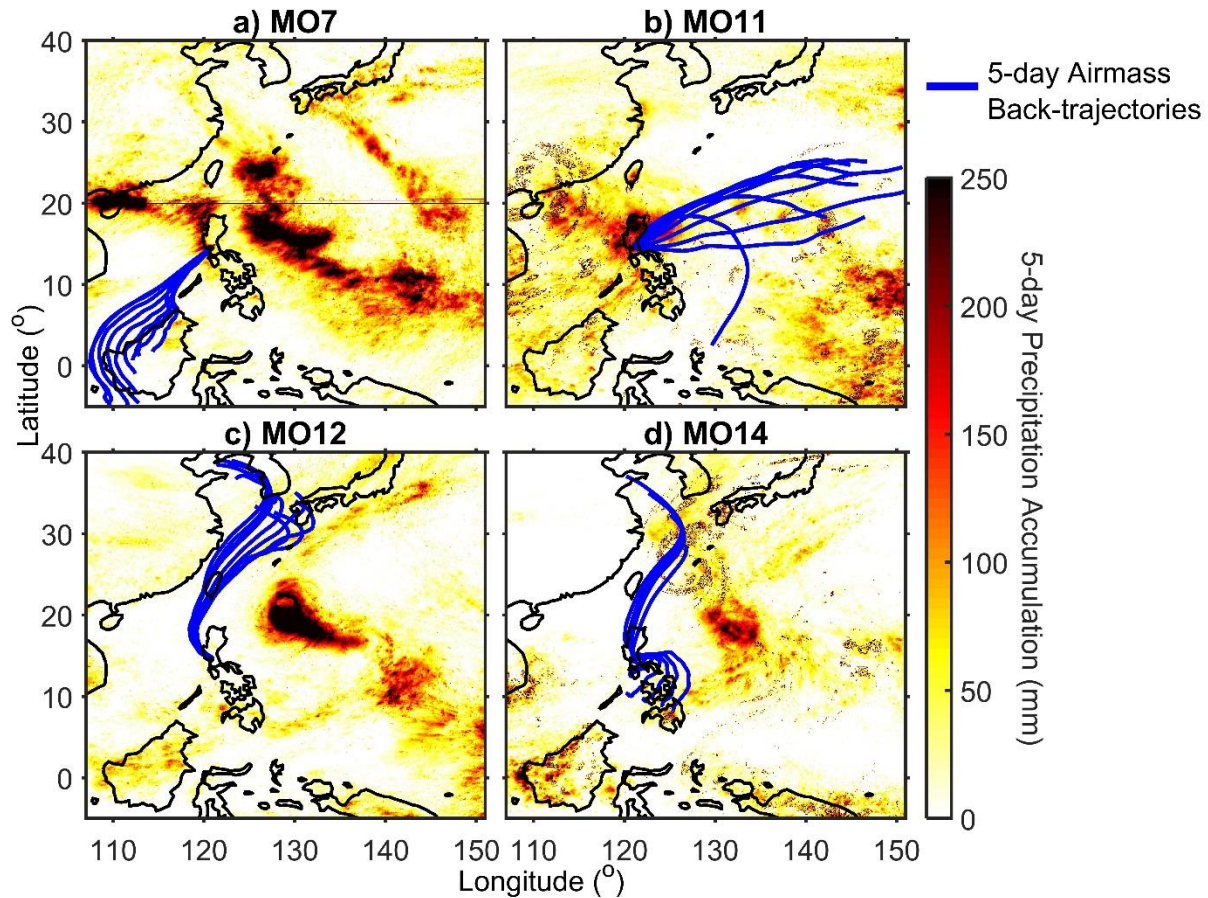
1243 **Table 1.** Description of the MOUDI sample sets from this study. Accumulated precipitation
 1244 during the sample sets was found using PERSIANN-CCS for the area bounded by: 121.0199 -
 1245 121.0968° E and 14.6067 - 14.6946° N.
 1246

Set Name	Start Date/ Local Time	End Date/ Local Time	Total Water-Soluble Species ($\mu\text{g m}^{-3}$)	% of water- soluble mass < 1 μm	Precipitation (mm)
MO1	7/19/18 12:40 PM	7/20/18 12:43 PM	4.61	67.3%	27
MO2	7/23/18 11:29 AM	7/25/18 5:10 PM	6.52	62.1%	14
MO4	7/25/18 7:16 PM	7/30/18 6:12 PM	5.17	66.4%	35
MO5	7/30/18 7:17 PM	8/1/18 1:19 PM	9.17	64.8%	11
MO6	8/6/18 2:33 PM	8/8/18 2:38 PM	5.11	55.8%	50
MO7	8/14/18 1:59 PM	8/16/18 2:04 PM	13.70	60.3%	3
MO8	8/22/18 1:46 PM	8/24/18 1:53 PM	12.73	71.6%	10
MO9	9/1/18 5:00 AM	9/3/18 5:05 AM	6.23	76.7%	64
MO10	9/10/18 2:42 PM	9/12/18 3:02 PM	6.36	79.5%	20
MO11	9/18/18 2:12 PM	9/20/18 2:24 PM	2.70	47.3%	26
MO12	9/26/18 1:53 PM	9/28/18 1:53 PM	13.49	59.9%	1
MO14	10/6/18 5:00 AM	10/8/18 5:05 AM	16.55	78.4%	0

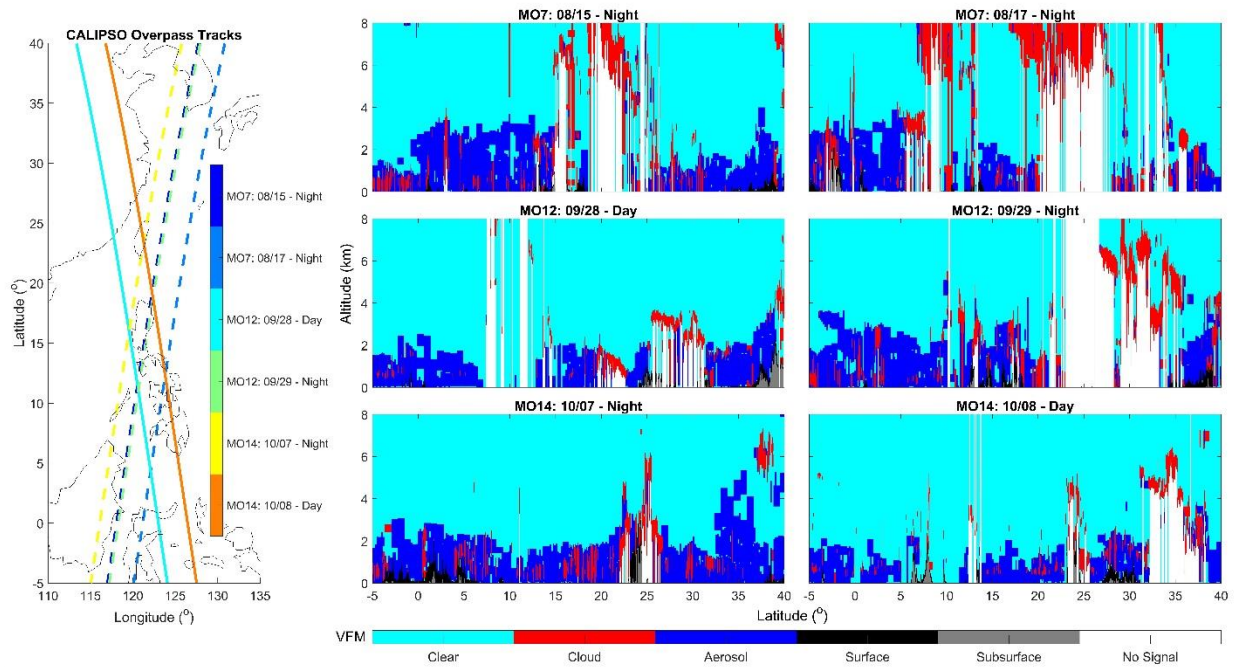


1247
 1248
 1249
 1250
 1251
 1252

Figure 1. MERRA-2 data for 850 hPa wind vectors and total cloud fraction averaged over the sample set duration for a) MO7 (8/14 – 8/16), b) MO11 (9/18 – 9/20), c) MO12 (9/26 – 9/28), and d) MO14 (10/6 – 10/8). The location of the Manila Observatory is indicated by the red circle. (Note that 850 hPa wind vectors are also averaged to increase grid spacing and improve figure readability.)

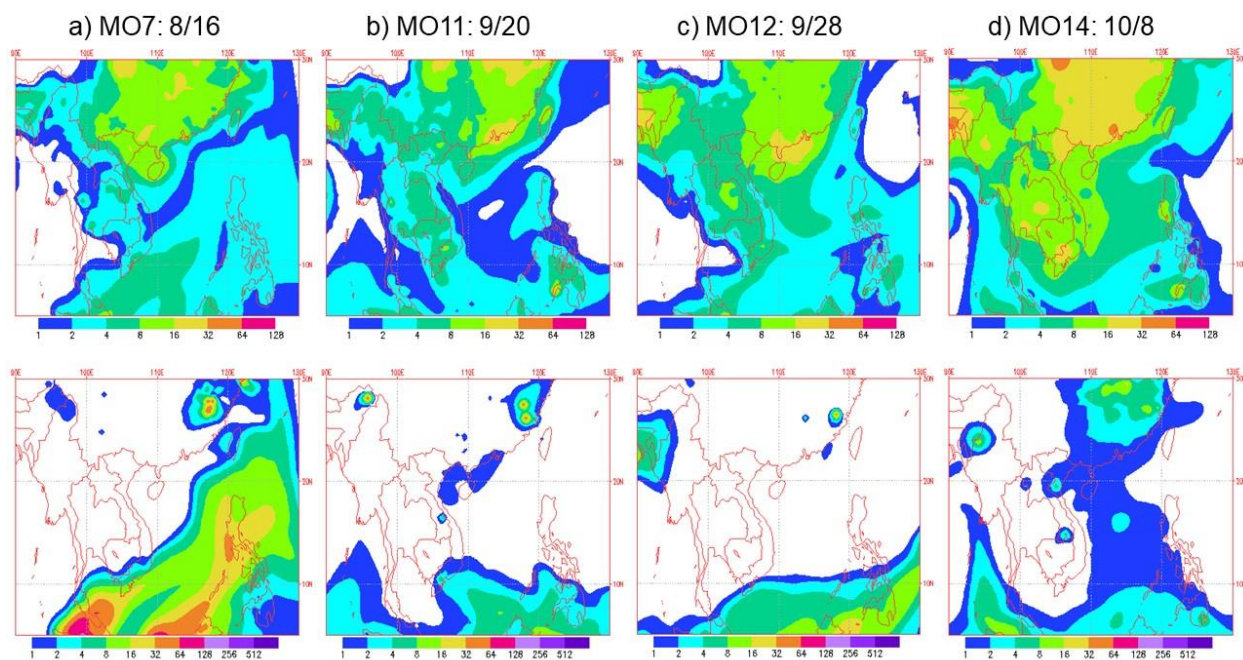


1253
 1254 **Figure 2.** Rainfall accumulation, extending from 5 days before the midpoint of each sample set
 1255 until the midpoint of each sample set, from PERSIAN-CCS for a) MO7, b) MO11, c) MO12, and
 1256 d) MO14. In blue are the 5-day air mass back-trajectories terminating at the MOUDI inlet at MO
 1257 (~85 m above sea level) every 6 h during each of the sample study periods. Note that the
 1258 maximum precipitation accumulation in the region shown during the study periods was 955 mm;
 1259 however, for figure readability, the scale was reduced to 0-250 mm.

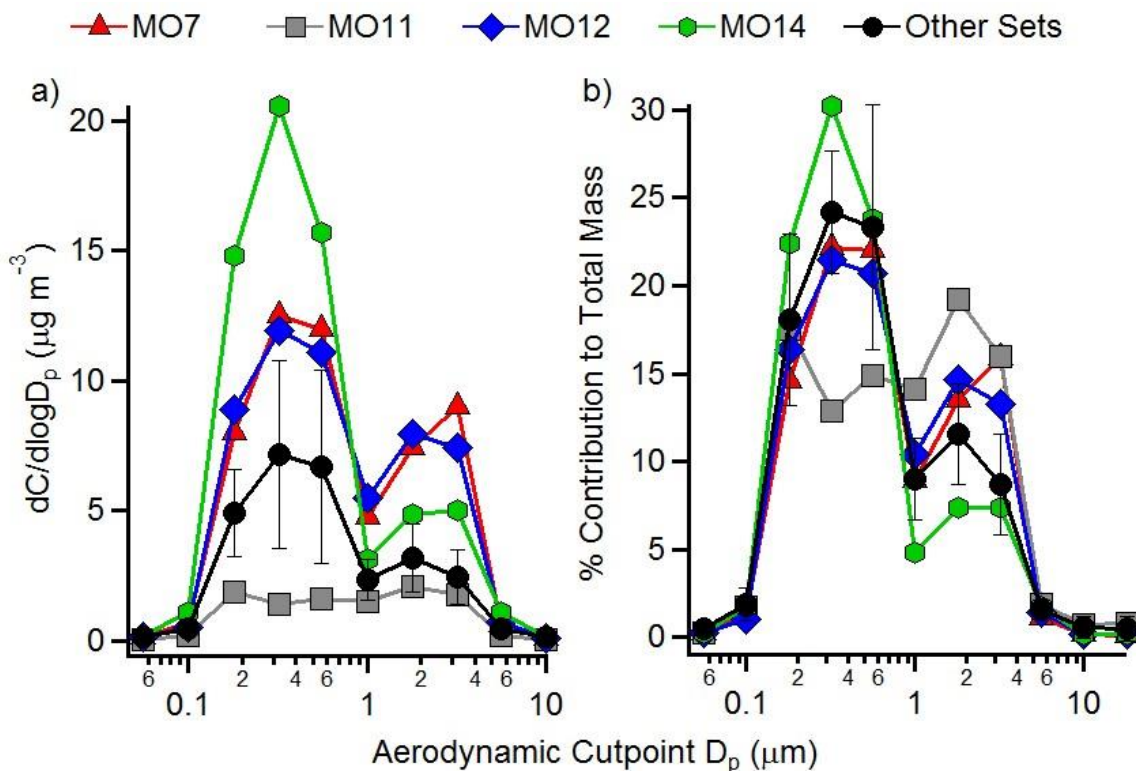


1260
 1261
 1262
 1263
 1264
 1265
 1266

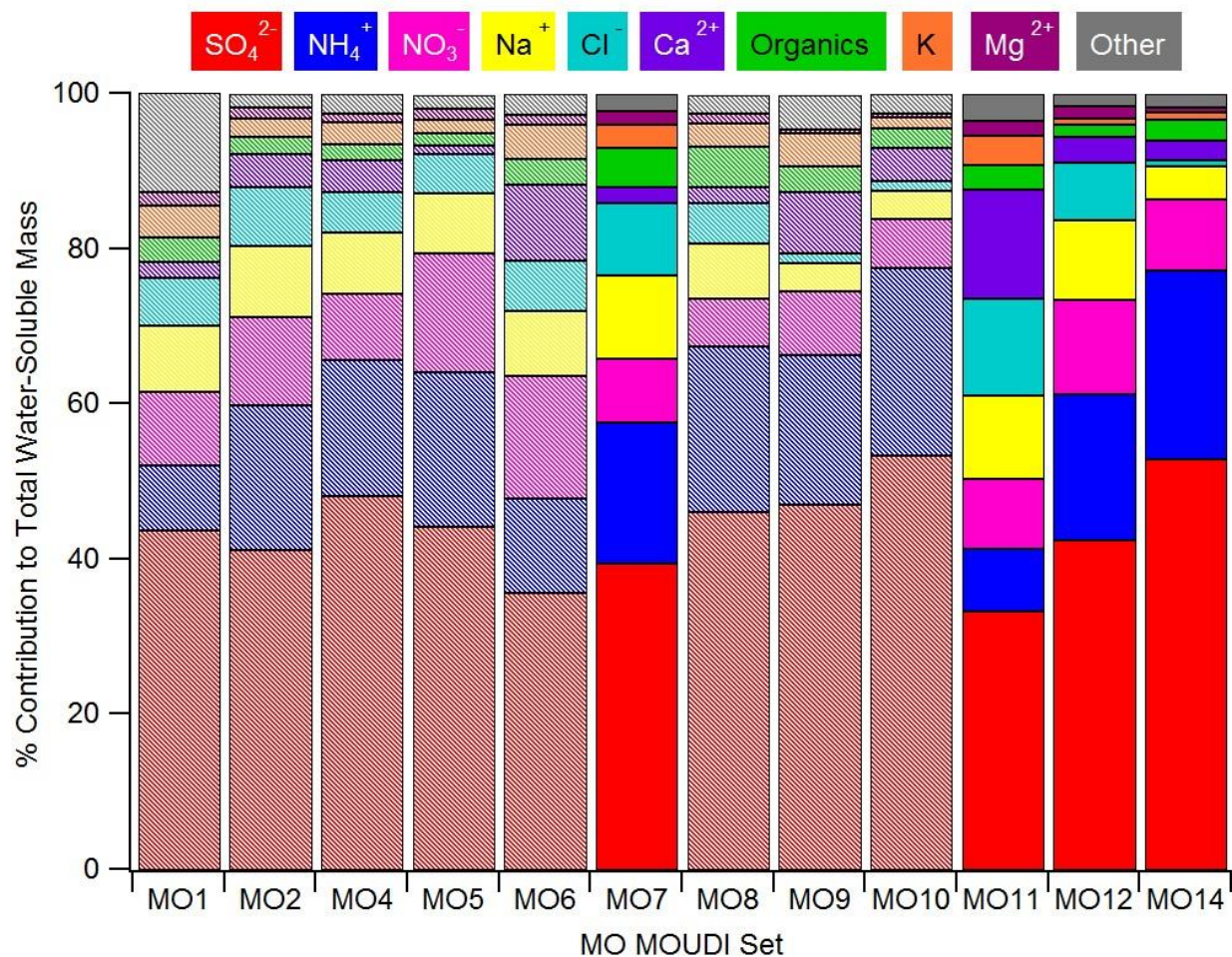
Figure 3. CALIOP Vertical Feature Mask (VFM) for overpasses during or following MO7, MO12, and MO14. For the CALIPSO satellite overpass tracks, the dashed lines correspond to the nighttime profiles and solid lines are for daytime. Note that nighttime overpasses correspond to early morning times before sunrise for the listed days and daytime overpasses occurred during early afternoon.



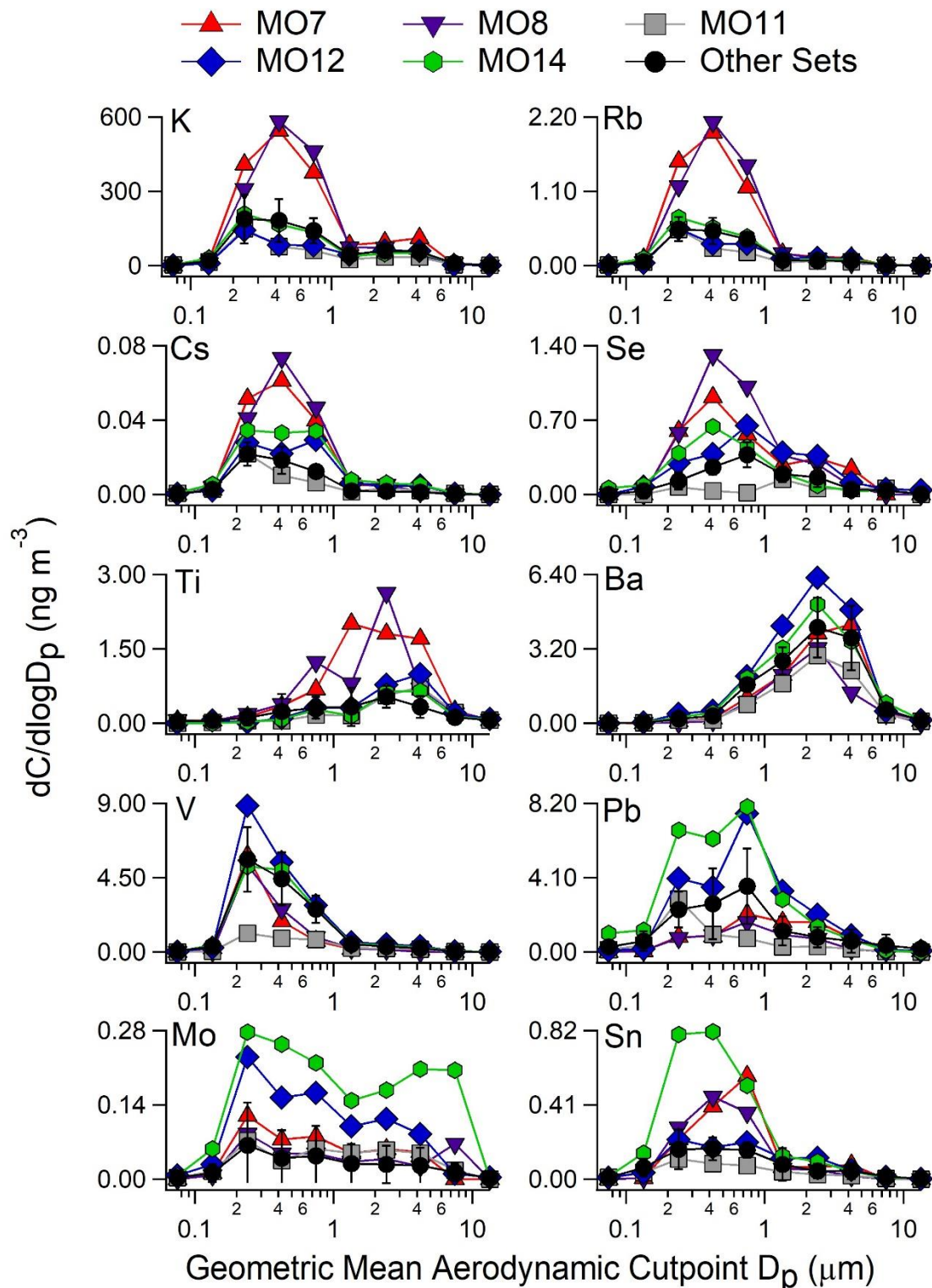
1267
 1268 **Figure 4.** NAAPS model snapshots corresponding to conditions at the stop time of sample sets a)
 1269 MO7, b) MO11, and c) MO12 and d) 3 h after the sample stop time for MO14. The top row of
 1270 figures is anthropogenic and biogenic fine aerosol (ABF) surface concentration ($\mu\text{g m}^{-3}$), while
 1271 the bottom row is biomass burning smoke surface concentration ($\mu\text{g m}^{-3}$).



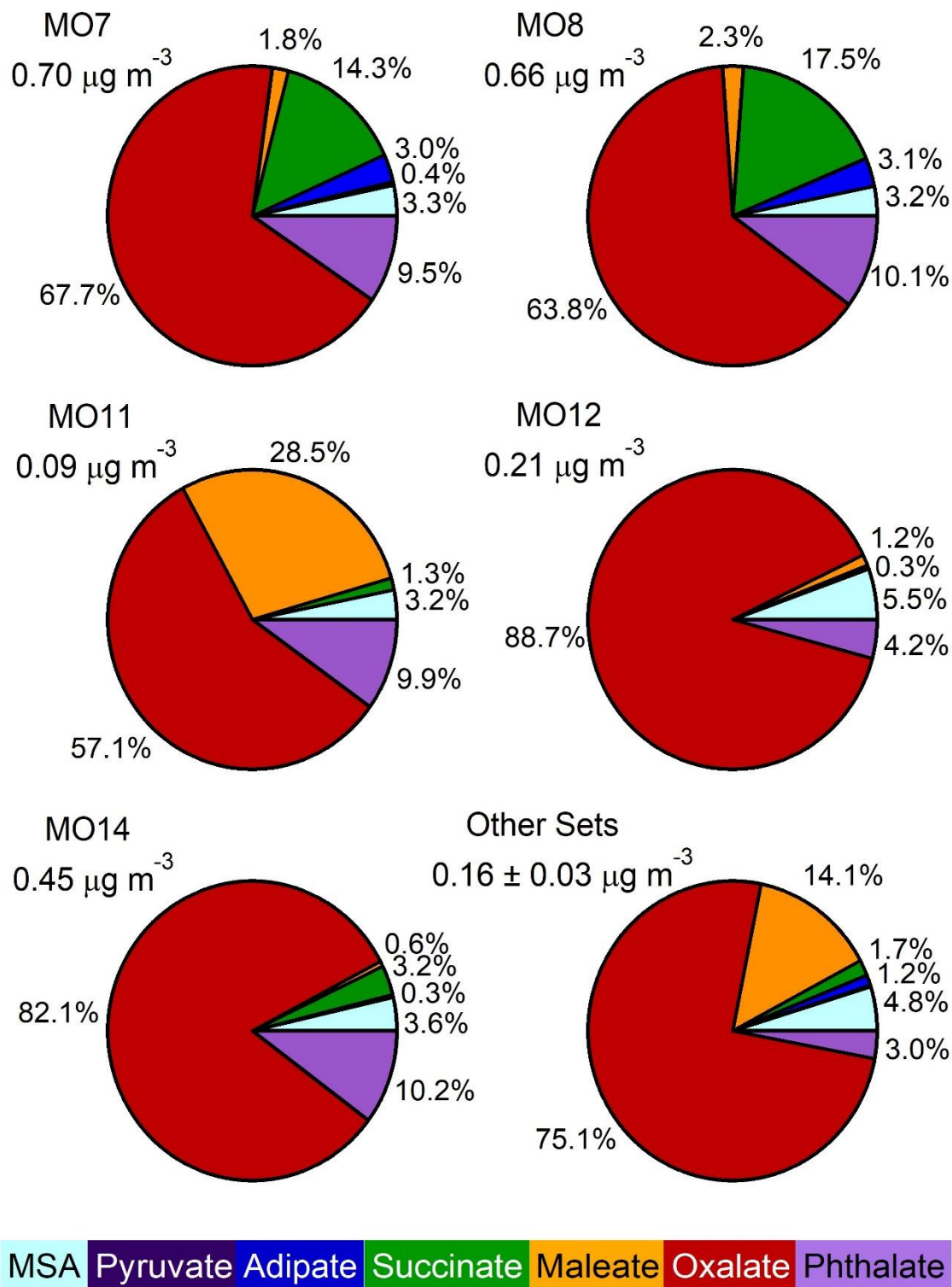
1272
 1273 **Figure 5.** a) Mass size distributions for total water-soluble mass ($C =$ sum of mass
 1274 concentrations for water-soluble species) and b) percent contribution of each size range to the
 1275 total water-soluble mass for the three MOUDI sets with the highest aerosol mass concentrations
 1276 (MO7, MO12, and MO14), the set with the lowest concentration (MO11), and the average (\pm one
 1277 standard deviation error bars) for the remaining eight sets.
 1278



1279
 1280 **Figure 6.** Percent contribution of various species to the total water-soluble mass concentration
 1281 for each of the 12 sample sets. The sample sets with the three highest aerosol concentrations
 1282 (MO7, MO12, and MO14) and the lowest aerosol concentration (MO11) are shown as solid bars
 1283 while all other sample sets are stripes. The “organics” category contains the sum of
 1284 methanesulfonate (MSA), pyruvate, adipate, succinate, maleate, oxalate, and phthalate.



1285
 1286 **Figure 7.** Selected elements that showed elevated concentrations during at least one of the
 1287 highest aerosol events (MO7, MO8, MO12, or MO14). The concentrations from the lowest
 1288 aerosol event (MO11) are also shown. The “other sets” category displays the average (\pm one
 1289 standard deviation) for the remaining seven sets.



1290
1291
1292
1293
1294
1295

Figure 8. Pie charts showing the fraction of species contributing to the measured water-soluble organic aerosol. Below each pie chart title is the sum of the water-soluble organic species measured, with the “other sets” chart showing the average \pm one standard deviation for the remaining sets. Acronyms: Methanesulfonate (MSA)